This Accepted Manuscript has not been copyedited and formatted. The final version may differ from this version.

eNeuro

Research Article: New Research | Disorders of the Nervous System

Blood-Brain Barrier Leakage during Early Epileptogenesis Is Associated with Rapid Remodeling of the Neurovascular Unit

Marion Bankstahl[1], Heike Breuer[1,2], Ina Leiter[1,2], Martin Märkel[3], Pablo Bascuñana[2], Dominik Michalski[4], Frank M. Bengel[2], Wolfgang Löscher[1], Martin Meier[5], Jens P. Bankstahl[2] and Wolfgang Härtig[3]

[1]*Department of Pharmacology, Toxicology and Pharmacy, University of Veterinary Medicine Hannover and Center for Systems Neuroscience, Bünteweg 17, Hannover, 30559, Germany*

[2]*Department of Nuclear Medicine, Hannover Medical School, Hannover, 30625, Germany*

[3]*Paul Flechsig Institute for Brain Research, University of Leipzig, Liebigstr. 19, Leipzig, 04103, Germany*

[4]*Department of Neurology, University of Leipzig, Liebigstr. 20, Leipzig, 04103, Germany*

[5]*Preclinical Imaging Labs, Central Laboratory Animal Facility & Institute for Laboratory Animal Science, Hannover Medical School, Hannover, 30625, Germany*

DOI: 10.1523/ENEURO.0123-18.2018

Received: 29 March 2018

Accepted: 1 April 2018

Published: 8 May 2018

Author Contributions: MB, JPB, DM, FMB, WL, and WH designed research; MB, HB, IL, MMä, MMe, JPB, and WH performed research; MB, HB, IL, PB, and JPB analyzed data; MB, JPB, and WH wrote the paper.

Funding: European Union Seventh's Frame Work Programme
602102

Conflict of Interest: Authors declare no conflict of interest.

This study was funded by the European Union Seventh's Framework Programme (FP7/2007-2013) under grant agreement n°602102 (EPITARGET). HB was supported by a scholarship from the Studienstiftung des Deutschen Volkes. IL was supported by a scholarship from the Konrad-Adenauer-Stiftung e.V.

J.P.B. and W.H. are contributed equally to this study.

Correspondence should be addressed to: Marion Bankstahl, University of Veterinary Medicine Hannover, Department of Pharmacology, Toxicology and Pharmacy, Bünteweg 17, D-30559 Hannover, Germany, Tel: +49-511-9538729, Fax: +49-511-9538581, E-mail: marion.bankstahl@tiho-hannover.de

Cite as: eNeuro 2018; 10.1523/ENEURO.0123-18.2018

Alerts: Sign up at eneuro.org/alerts to receive customized email alerts when the fully formatted version of this article is published.

Accepted manuscripts are peer-reviewed but have not been through the copyediting, formatting, or proofreading process.

Copyright © 2018 Bankstahl et al.
This is an open-access article distributed under the terms of the Creative Commons Attribution 4.0 International license, which permits unrestricted use, distribution and reproduction in any medium provided that the original work is properly attributed.

eNeuro Accepted Manuscript

eNeuro Accepted Manuscript

1. Title: Blood-brain barrier leakage during early epileptogenesis is associated with rapid remodeling of the neurovascular unit

2. Abbreviated title: Neurovascular unit during epileptogenesis

3. Author names: Marion Bankstahl[1*], Heike Breuer[1,2], Ina Leiter[1,2], Martin Märkel[3], Pablo Bascuñana[2], Dominik Michalski[4], Frank M. Bengel[2], Wolfgang Löscher[1], Martin Meier[5], Jens P. Bankstahl[2#], Wolfgang Härtig[3#]

Author affiliations:

1 Department of Pharmacology, Toxicology and Pharmacy, University of Veterinary Medicine Hannover and Center for Systems Neuroscience, Bünteweg 17, 30559 Hannover, Germany

2 Department of Nuclear Medicine, Hannover Medical School, 30625 Hannover, Germany

3 Paul Flechsig Institute for Brain Research, University of Leipzig, Liebigstr. 19, 04103 Leipzig, Germany

4 Department of Neurology, University of Leipzig, Liebigstr. 20, 04103 Leipzig, Germany

5 Preclinical Imaging Labs, Central Laboratory Animal Facility & Institute for Laboratory Animal Science, Hannover Medical School, 30625 Hannover, Germany

4. Author Contributions: MB, JPB, DM, FMB, WL, and WH designed research; MB, HB, IL, MMä, MMe, JPB, and WH performed research; MB, HB, IL, PB, and JPB analyzed data; MB, JPB, and WH wrote the paper.

5. *Correspondence should be addressed to: Marion Bankstahl, University of Veterinary Medicine Hannover, Department of Pharmacology, Toxicology and Pharmacy, Bünteweg 17, D-30559 Hannover, Germany, Tel: +49-511-9538729, Fax: +49-511-9538581, E-mail: marion.bankstahl@tiho-hannover.de

[#]These authors contributed equally to this study.

eNeuro Accepted Manuscript

24 **6. Number of figures:** 10

25 **7. Number of tables:** 2

26 **8. Number of multimedia:** 0

27 **9. Number of words for abstract:** 244

28 **10. Number of words for significance statement:** 100

29 **11. Number of words for introduction:** 493

30 **12. Number of words for discussion:** 2137

31 **13. Acknowledgements:** We are grateful to Johannes Kacza, Jens Grosche, Bianca Mages, Christian

32 Bergen, Nathalie Hildebrandt, Annika Thomer, and Friederike Twele for excellent assistance.

33 **14. Conflict of interest:** The authors declare no competing financial interests.

34 **15. Funding sources:** This study was funded by the European Union Seventh's Framework

35 Programme (FP7/2007-2013) under grant agreement n°602102 (EPITARGET). HB was supported by a

36 scholarship from the Studienstiftung des Deutschen Volkes. IL was supported by a scholarship from

37 the Konrad-Adenauer-Stiftung e.V..

eNeuro Accepted Manuscript

38 **Abstract**

39 Increased permeability of the blood-brain barrier (BBB) following cerebral injury results in regional
40 extravasation of plasma proteins and can critically contribute to the pathogenesis of epilepsy. Here,
41 we comprehensively explored the spatiotemporal evolution of a main extravasation component,
42 albumin, and illuminate associated responses of the neurovascular unit (NVU) contributing to early
43 epileptogenic neuropathology. We applied translational *in vivo* MR imaging and complementary
44 immunohistochemical analyses in the widely used rat pilocarpine-post status epilepticus (SE) model.
45 The observed rapid BBB leakage affected major epileptogenesis-associated brain regions, peaked
46 between 1 and 2 days post SE, and rapidly declined thereafter, accompanied by cerebral edema
47 generally following the same time course. At peak of BBB leakage,serum albumin colocalized with
48 NVU constituents, like vascular components, neurons and brain immune cells. Surprisingly, astroglial
49 markers did not colocalize with albumin and aquaporin-4 (AQP4) was clearly reduced in areas of
50 leaky BBB, indicating a severe disturbance of astrocyte-mediated endothelial-neuronal coupling. In
51 addition, a distinct adaptive reorganization process of the NVU vasculature apparently takes place at
52 sites of albumin presence, substantiated by reduced immunoreactivity of endothelial and changes in
53 vascular basement membrane markers. Taken together, degenerative events at the level of the NVU,
54 affecting vessels, astrocytes and neurons, seem to outweigh reconstructive processes. Considering
55 the rapidly occurring BBB leakage and subsequent impairment of the NVU, our data support the
56 necessity of a prompt BBB-restoring treatment as one component of rational therapeutic
57 intervention to prevent epileptogenesis and the development of other detrimental sequelae of SE.

58

59 **Significance statement**

60 Blood-brain barrier (BBB) leakage is critically involved in brain insult-mediated epilepsy development.
61 Here, we demonstrate rapid but transient BBB damage within hours after experimental status
62 epilepticus (SE), an epileptogenic insult, and subsequent degenerative events at the level of the so

eNeuro Accepted Manuscript

63 called neurovascular unit (NVU), which reflects the anatomical and functional interplay between
64 brain vasculature, glial cells and neurons. Analyses at cellular level revealed degeneration of various
65 NVU components, which seem to outweigh reconstructive processes, thus providing potential targets
66 for protective pharmacotherapy. The findings emphasize the requirement and expedience of rapid
67 BBB-stabilizing treatment as a primary element of epilepsy-preventive therapeutic interventions.
68
69
70

eNeuro Accepted Manuscript

71 **Introduction**

72 Different kinds of cerebral injury, like head trauma, stroke, cerebral infection, or status epilepticus
73 (SE) may lead to the development of epilepsy in a certain proportion of affected patients (Pitkänen
74 and Immonen, 2014; Schmidt and Sillanpää, 2016). The mechanisms subjacent to the process of
75 epileptogenesis following brain insults, though, are not well understood. One common characteristic
76 of epileptogenic brain insults is an impairment of the blood-brain barrier (BBB). A leakage of the BBB
77 results in extravasation of albumin and subsequent activation of glia and inflammatory responses
78 and is considered as one likely key factor triggering epileptogenesis (Seiffert et al., 2004; Ivens et al.,
79 2007; van Vliet et al., 2007; Marcon et al., 2009).

80 Albumin extravasation into the brain, eventually resulting in recurrent electrographic seizures (Bar-
81 Klein et al., 2014; Weissberg et al., 2015), is observed in various post-SE models of epileptogenesis
82 (van Vliet et al., 2007; Michalak et al., 2013; Breuer et al., 2016). Importantly, increased BBB
83 permeability is currently under investigation as potential prognostic biomarker for stratifying
84 individuals at risk to develop epilepsy following epileptogenic brain insults (Pitkänen et al., 2016;
85 Walker et al., 2016, Bar-Klein et al., 2017) and as treatment target for attenuation or prevention of
86 epileptogenesis by applying drugs stabilizing or restoring BBB function during the latency phase
87 preceding appearance of the first clinical seizure (Friedman and Heinemann, 2012; Janigro, 2012; van
88 Vliet et al., 2016). For both objectives, it is crucial to reveal the *in vivo* spatiotemporal pattern of BBB
89 leakage following cerebral injury. Furthermore, elucidating cellular and parenchymal distribution
90 patterns of extravasated serum albumin and associated changes in the neurovascular unit (NVU) will
91 be beneficial for better understanding of pathological cascades finally leading to chronic seizure
92 generation. In view of the broad application of the pilocarpine rat model, which is one of the most
93 widely used rodent models of epileptogenesis and has brought a large body of information relevant
94 to epilepsy development and its prevention, we consider it important to further characterize this
95 model. Moreover, recent studies in a refined version of this model (Bröer et al., 2016, Brandt et al.,
96 2015) argue for its beneficial application for predictive biomarker identification. Further, severe SE

eNeuro Accepted Manuscript

97 itself is a common and life-threatening neurological condition. Understanding its consequences is of
98 high importance, also considering its induction by cholinergic nerve agents released by chemical
99 weapons (Tang et al., 2011).

100 Therefore, we here firstly present detailed data on the *in vivo* spatiotemporal pattern of BBB leakage
101 during epileptogenesis in the lithium-pilocarpine-post-SE model of epileptogenesis in rats assessed
102 by contrast-enhanced MR imaging for which we recently published a methodological paper
103 identifying the most suitable translational imaging approach (Breuer et al., 2016). Secondly, the
104 cellular uptake and extracellular distribution pattern of fluorescein-linked albumin were determined.
105 Thirdly, multiple fluorescence staining was applied to identify colocalization of extravasated serum
106 albumin with various histochemical markers for cellular and acellular constituents of the extended
107 NVU, i.e. BBB endothelium, the vascular basement membranes, the glia-endothelial interface,
108 astrocytes, microglia, and neurons.

109

110 **Material and Methods**

111 **Animals**

112 Adult female Sprague Dawley rats (200-220 g, n = 60) were obtained from Harlan Laboratories. They
113 were housed in pairs under controlled climate conditions (22±1°C, humidity 45-55%) in individually
114 ventilated cages under a 14/10 h light-dark cycle (rats used for imaging experiments), or in groups of
115 5 in open cages (22±1°C, humidity 45-55%) under a 12/12 h light-dark cycle (rats used for
116 immunohistochemistry). Standard diet (Altromin 1324; Altromin, Lage, Germany) and water were
117 accessible *ad libitum*. After delivery, animals were allowed to adapt to the new conditions, were
118 repetitively handled for at least one week before being subjected to experiments, and randomized to
119 experimental groups. Experiments were conducted in accordance with European Communities
120 Council Directives 86/609/EEC and 2010/63/EU and were formally approved by the responsible local
121 authority.

eNeuro Accepted Manuscript

122 **Chemicals, drugs, and antibodies**

123 Isoflurane (Isofluran Baxter) was obtained from Baxter (Unterschleißheim, Germany) and CP-Pharma
124 (Burgdorf, Germany), diazepam as commercial solution (Faustan or Diazepam-ratiopharm) from
125 Temmler Pharma GmbH (Marburg, Germany) or Ratiopharm (Ulm, Germany), respectively, and
126 glucose electrolyte solution (Sterofundin HEG-5) from B. Braun (Melsungen, Germany). Gadolinium-
127 DTPA (Gd-DTPA, Magnevist 0.5 mmol/ml) was purchased from Bayer HealthCare (Leverkusen,
128 Germany). All immunoreagents were obtained from Dianova (Hamburg, Germany) as supplier for
129 Jackson ImmunoResearch (West Grove, PA, USA). Unless stated otherwise, all further chemicals were
130 of analytic grade and purchased from Sigma-Aldrich (Schnelldorf, Germany).

131 **Induction of status epilepticus**

132 SE was induced in rats (n=42) as described elsewhere (Bankstahl et al., 2012). Shortly, 14–16 h after
133 the administration of lithium chloride (127 mg/kg in 3 ml/kg 0.9% saline, p.o.) and 30 min after
134 methyl scopolamine (1 mg/kg in 2 ml/kg 0.9% saline, i.p.), injection of pilocarpine (10 mg/kg,
135 repeated up to 5 times, in 1 ml/kg 0.9% saline, i.p.) was repeated until SE, which was characterized
136 by the onset of repetitive generalized convulsive seizures (stage 4 or 5) without intermediate
137 recovery of normal behavior. SE was interrupted after 90 min by administration of diazepam (10
138 mg/kg in 2 ml/kg, i.p.). Diazepam injection was repeated after 15 min (10 mg/kg), and, if needed,
139 after 30 min using half of the first dose (5 mg/kg). Self-sustaining SE successfully established in 90.5%
140 of animals, which required an average pilocarpine dose of 35.4 ± 9.6 mg/kg (mean ± SD). Three rats
141 in which SE could not be induced served as additional control group for albumin extravasation. The
142 overall mortality rate was zero. Age-matched control rats (n = 10) for histological analysis were
143 treated identically but received saline instead of pilocarpine. After SE, rats were hand-fed with
144 mashed laboratory chow and received injections of glucose-electrolyte solution until they resumed
145 normal feeding behavior.

146 **Magnetic resonance imaging**

eNeuro Accepted Manuscript

147 Rats were scanned before (baseline, n = 13) and 48 h (n = 5), 4 days (n = 6), and 10 days (n = 5)
148 following SE. MRI was conducted as described recently (Breuer et al., 2016) on a 7 T (300 MHz) small
149 animal MRI system (Bruker Pharmascan) using ParaVision 5.1 acquisition software (Bruker, Ettlingen,
150 Germany). Rats were anesthetized with isoflurane and a catheter was placed in a lateral tail vein for
151 contrast agent infusion. Following transfer of rats into the imaging chamber, which was constantly
152 kept at 37°C, the rat maxilla was placed in a tooth bar for comparable positioning. The receive coil
153 was placed at a defined position over the rat head. Breathing rate of rats during image acquisition
154 was kept at 40 to 60 breaths/min. T2-weighted 2D multi slice multi echo images (MSME; repetition
155 time=2500 ms, echo time=11 ms, 96 slices of 0.8 mm, 256x256 matrix, 35x35x25.6 mm^3 field of view)
156 were acquired for detection of brain edema. T1-weighted images were acquired using a 3D modified
157 driven equilibrium Fourier transform method (MDEFT; 0.8 mm slice thickness, 256x256x32 matrix,
158 35x35x25.6 mm^3 field of view) before and 30 min after start of contrast agent infusion. The resulting
159 voxel size was 0.136x0.136x0.8 mm^3. Gd-DTPA was intravenously infused via a syringe pump (PHD
160 Ultra, Harvard Apparatus, South Natick, MA, USA) utilizing a 20 min step-down infusion schedule as
161 described recently (Breuer et al., 2016).

162 **Image analysis**

163 MRI data were co-registered to a rat brain atlas published by Schwarz et al. (2006) using PMOD
164 software (PMOD Technologies Ltd., Zurich, Switzerland), and data from six brain regions
165 (hippocampus, thalamus, amygdala, piriform cortex, entorhinal cortex, and cerebellum) were
166 extracted. T1- and T2 signals were normalized to pons, for which no alterations in contrast agent
167 uptake or T2 MRI signal was observed after SE (Breuer et al., 2016). Voxelwise comparison to
168 baseline (two-sample unpaired t-test, significance level threshold: 0.001, minimum cluster size: 100
169 voxels) led to Gd-DTPA leakage t-maps using MATLAB software (MathWorks, Natick, MA, USA) and
170 SPM12 (UCL, London, UK) as described earlier (Breuer et al., 2016).

171 **FITC-albumin infusion and brain slicing**

eNeuro Accepted Manuscript

172 For histological analysis of albumin extravasation, rats were infused with 100 mg/kg bovine albumin-
173 fluorescein isothiocyanate conjugate (FITC-albumin) diluted in 10 ml/kg 0.1 M phosphate buffered
174 saline (PBS) at a rate of 1 ml/min under short isoflurane anesthesia without prior SE (control, n = 10),
175 and 5 h (n = 6), 24 h (n = 5), or 48 h following SE (n = 16). Two hours later, rats were perfused with
176 125 ml 0.01 M PBS followed by 250 ml of 4% paraformaldehyde in 0.1 M PBS at a flow rate of 16.6
177 ml/min. Following removal, brains were kept for 24 h in 4% phosphate-buffered paraformaldehyde
178 for post-fixation and were then stored in 30% sucrose in 0.1 M PBS with 0.2% sodium azide at 4°C
179 until sectioning. Coronal sectioning of the forebrain of each rat was performed using a freezing
180 microtome (Frigomobil 1205; Jung, Heidelberg, Germany) and a slice thickness of 30 µm. For analysis
181 of FITC-albumin extravasation patterns, series comprising each 10th coronal serial section from the
182 forebrains of all rats were washed 3 times with TBS for at least 10 min, briefly rinsed with distilled
183 water, mounted onto fluorescence-free slides (Menzel, Braunschweig, Germany), air-dried and cover
184 slipped with Entellan (Merck, Darmstadt, Germany).

185 **Semi-quantitative analysis of extra- and intracellular FITC-albumin**

186 The extent of extracellular and cellular FITC-albumin uptake was scored blinded to experimental
187 groups. Whole brain slice images were acquired using an all-in-one fluorescence microscope
188 (Biorevo, BZ-9000E, Keyence). Four coronal brain sections were analyzed per animal (-0.36 mm, -1.56
189 mm, -3.72 mm and -4.9 mm relative to bregma) (Paxinos and Watson, 2007). Target regions were
190 hippocampus, thalamus, amygdala, piriform cortex, entorhinal cortex, and caudate putamen. Scoring
191 was performed separately for cellular and extracellular FITC-albumin occurrence: (1) cellular FITC-
192 albumin uptake: score 0, no cellular uptake, score 1, sporadic cellular uptake, score 2, medium
193 amount of labeled cells, brain region is only affected in parts, score 3, high amount of labeled cells,
194 brain region is globally affected; (2) extracellular FITC-albumin uptake: score 0, no extracellular FITC-
195 albumin, score 1, minimal extracellular uptake, often near to blood vessels, score 2, medium
196 extracellular FITC-albumin accumulation, rather focal, score 3, high-grade extracellular FITC-albumin

eNeuro Accepted Manuscript

197 accumulation, rather global. Target regions were scored in both hemispheres and means of left and
198 right and of the four section levels were calculated.

199 Quantification of albumin extravasation following conversion into a light microscopically visible
200 adduct

201 The immunohistochemical conversion of the FITC-albumin signal into a light microscopically visible
202 adduct based on an anti-fluorescein-horseradish peroxidase (HRP) conjugate (Dianova) and nickel-
203 enhanced diaminobenzidine (DAB-Ni) as chromogen for the marker enzyme. For this conversion,
204 serial sections were extensively rinsed with TBS followed by abolishing of endogenous peroxidase
205 activity within the tissue by treatment with 0.6% hydrogen peroxide in TBS for 30 min. After 3 further
206 rinses with TBS for 10 min each, non-specific binding sites for the immunoreagent were blocked with
207 TBS containing 2% bovine serum albumin and 0.3% Triton X-100 (TBS-BSA-T) for 30 min.
208 Subsequently, all sections were incubated with anti-fluorescein-HRP (1:2000 in TBS-BSA-T) for 2 h.
209 Next, the sections were rinsed twice with TBS and once with 0.05 M Tris buffer, pH 8, for 10 min
210 each. The sections were then stained by reacting for 4 min with a DAB-Ni solution (containing 40 mg
211 nickel ammonium sulfate, 2 mg DAB tetrahydrochloride and 5 µl of hydrogen peroxide (30%) in 10 ml
212 of 0.05 M Tris buffer, pH 8).

213 For quantification of FITC-albumin extravasation, images of whole brain sections were acquired at -
214 0.36 mm, -1.56 mm, -3.72 mm, and -4.90 mm relative to bregma by a Keyence microscope and
215 analyzed with an image quantification software (Volocity 4.3.2, PerkinElmer, Waltham, MA, USA).
216 Stained areas were calculated by the total number of pixels in the stained area relative to the total
217 area of the respective brain section as described recently (Michalski et al., 2010).

218 Multiple fluorescence staining

219 Furthermore, selected FITC-albumin-pre-labeled sections were applied to double fluorescence
220 staining. For this purpose, the sections were extensively rinsed with TBS prior to blocking of
221 unspecific binding sites with TBS containing 5% normal donkey serum and 0.3% Triton X-100 (TBS-

eNeuro Accepted Manuscript

222 NDS-T). The sections were then applied to mixtures of antibodies or of antibodies and lectins as listed
223 in Table 1. Thereby, all markers were diluted in TBS-NDS-T, and in general the incubation time was 20
224 h at room temperature. Three rinses with TBS for 10 min each were followed by incubation with
225 cocktails of carbocyanine (Cy)3- and Cy5-conjugated immunoreagents, which were used at 20 µg/ml
226 TBS-BSA for 1 h. The omission of primary antibodies and lectins in histological control experiments
227 resulted in the expected absence of any cellular fluorescence labeling. Pictures at lower
228 magnifications for Fig. 2 B and D were acquired with a Keyence microscope BZ 9000, all other
229 pictures with a confocal laser scanning microscope LSM 510 Meta from Zeiss (Göttingen, Germany).

230 **Assessment of neurodegeneration**

231 Assessment of neurodegeneration was performed in Nissl-stained coronal brain sections in a blinded
232 fashion with respect to the time point following SE. First, severity of neuronal damage was semi-
233 quantitatively assessed by a grading system as previously described (Bankstahl et al., 2012): score 0,
234 no obvious damage; score 1, slightly abnormal appearance of the structure without clear evidence of
235 visible neuronal loss; score 2, lesions involving 20–50% of neurons; score 3, lesions involving >50% of
236 neurons. Scoring was performed in hippocampal subregions (CA1, CA3a), amygdala, and piriform and
237 entorhinal cortex in four sections per rat (−2.4 mm, −3.36 mm, -4.68 mm, and −5.64 mm relative to
238 bregma according to Paxinos and Watson, 2007). Averaged scores from these sections of both
239 hemispheres in each rat were used for calculation of group data. Second, the amount of polymorph
240 neurons in the dentate hilus was quantified as described earlier (Polascheck et al., 2010) using
241 AxioVision software (Zeiss). The dentate hilus was defined as the inner border of the granule cell
242 layer and two straight lines connecting the tips of the granule cell layer and the proximal end of the
243 CA3c region. Only cells of neuronal morphology and a diameter larger than 8 µm were counted. Per
244 rat, three sections (at −2.4 mm, −3.36 mm, and −4.68 mm relative to bregma) were analyzed and
245 numbers of neurons were averaged from these sections.

246 **Statistical analysis**

eNeuro Accepted Manuscript

247 Statistical analyses were performed using Prism 7 software (GraphPad Software, La Jolla, CA, USA).
248 Depending on whether data were normally distributed or not, either parametric or non-parametric
249 tests were used for statistical evaluation. All rank or score data were analyzed by non-parametric
250 tests. MRI data and data resulting from quantitative histological analysis were analyzed by one-way
251 analysis of variance (ANOVA), followed by Dunnett's multiple-comparison test comparing baseline to
252 each time point after SE. Non-parametric data resulting from semi-quantitative analysis of
253 immunohistochemical staining were analyzed by Kruskal–Wallis ANOVA, followed by Dunn's post-hoc
254 test comparing the control group with the SE groups at each time point. All tests were used two-
255 sided. If not stated otherwise, values of $p < 0.05$ were considered statistically significant.

256 **Results**

257 ***In vivo* spatiotemporal pattern of blood-brain barrier leakage during early epileptogenesis**

258 To determine the time course of BBB impairment during epileptogenesis, rats were scanned prior to
259 and at 5 h, 48 h, 4 days, and 10 days post SE using recently published contrast-enhanced T1-weighted
260 as well as T2-weighted MRI sequences (Breuer et al., 2016).

261 Gd-DTPA extravasation, resulting in elevated T1 values and indicating BBB leakage, was absent at
262 baseline and at 5 h post SE in all investigated brain regions (Fig. 1 A,B). Strongly increased T1 values
263 *versus* baseline were present 48 h post SE in epileptogenesis-associated brain regions ($p < 0.0001$ for
264 all brain regions), but not in the cerebellum (Fig. 1 B). The maximal signal enhancement occurred in
265 the amygdala with a T1 intensity increase of 221%. At 4 and 10 days post SE, a much lower but still
266 significant Gd-DTPA leakage was only detected in the amygdala (day 4, $p = 0.040$), piriform (day 4, $p =$
267 0.016, day 10, $p = 0.0036$) and entorhinal (day 10, $p = 0.030$) cortex, proposing a recovery of BBB
268 integrity in the other formerly affected brain regions (Fig. 1 B). Elevated T2 values, indicative of brain
269 edema, were present at 48 h post SE in all investigated brain regions including cerebellum ($p < 0.045$
270 for all brain regions) with the highest T2 value increase of 23% in the amygdala (Fig. 1 C,D). At 4 days
271 post SE, T2 values were still increased in hippocampus ($p = 0.035$), thalamus ($p = 0.011$), and

eNeuro Accepted Manuscript

272 entorhinal cortex ($p = 0.021$). Subsequently, edema further decreased and no significantly changed
273 T2 values were present at 10 days following SE (Fig. 1D).

274 **Extent and spatiotemporal pattern of FITC-albumin extravasation following status epilepticus**
275 **evaluated by histological analyses**

276 Histological analysis of DAB-converted FITC-albumin signals revealed distinct extravasation in
277 thalamic areas, amygdala, piriform and entorhinal cortices (Fig. 2A). Quantification of stained area
278 showed significantly elevated extravasation in thalamus at 24 ($p = 0.0017$) and 48 h post SE ($p =$
279 0.0028), whereas in amygdala and piriform/entorhinal cortex, significantly increased values were
280 found at all investigated time points (5 h, $p = 0.038$, 24 h, $p = 0.0001$, 48 h, $p = 0.013$; Fig. 2B). The
281 hippocampus was moderately affected only in individual animals, but signal quantification did not
282 reach statistical significance on group level (data not shown). Comparison of *ex vivo* extravasation
283 pattern (Fig. 2A) with *in vivo* contrast-enhanced MRI leakage map revealed a very comparable spatial
284 distribution of albumin 48 h post SE (Fig. 2C). Intra- and extracellular distribution of extravasated
285 FITC-albumin differed between individuals (Fig. 2D), but semiquantitative histological group analysis
286 of native FITC-albumin signal revealed extracellular FITC-albumin in thalamus ($p = 0.025$), amygdala
287 ($p = 0.0019$), piriform cortex ($p = 0.034$), entorhinal cortex ($p = 0.014$), and caudate putamen ($p =$
288 0.0063) already at 5 h following SE (Fig. 2E). At 24 h post SE, extracellular FITC-albumin reached its
289 maximum in all analyzed brain regions ($p \leq 0.0011$), and declined again at 48 h post SE (Fig. 2E). At 5
290 h following SE, intracellular FITC-albumin was observed only in amygdala ($p = 0.0015$) and entorhinal
291 cortex ($p = 0.045$), whereas it was found in all analyzed brain regions ($p \leq 0.022$) at 24 h following SE
292 (Fig. 2F). At 48 h following SE, it still reached significance in hippocampus ($p = 0.0048$), thalamus ($p =$
293 0.0017), and piriform cortex ($p = 0.0006$; Fig. 2F). In brain slices of control rats, neither extra- nor
294 intracellular FITC-albumin was observed. Furthermore, FITC-albumin leakage was not visible in
295 pilocarpine-treated rats without SE development (data not shown).

296 **Time course and extent of neurodegeneration following status epilepticus**

eNeuro Accepted Manuscript

297 Semi-quantitative analysis of neurodegeneration in hippocampal and cortical subregions as well as
298 amygdala revealed neuronal loss (exemplarily shown in Fig. 3A) already at 24 h following SE in the
299 amygdala (24 h, p = 0.018, 48 h, p = 0.0018) and the piriform and entorhinal cortices (24 h, p =
300 0.0097; Fig. 3C). At 48 h after SE, also hippocampal pyramidal cells of CA3c subregion reached
301 statistical significance (p = 0.017; Fig. 3C). Moreover, the number of hilar mossy cells and
302 interneurons as assessed by cell counting was significantly reduced at 48 h following SE (p = 0.026;
303 Fig. 3B).

304 **Colocalization of FITC-albumin with cellular or extracellular cerebral markers**

305 Randomly selected sections from rats 24 h and 48 h after SE were applied to multiple fluorescence
306 labeling. FITC-albumin, counterstained with biotinylated anti-NeuN (Fig. 4A’), displayed only minor
307 colocalization (Fig. 4A’’’), despite intracellular location of FITC-albumin in cells of obvious neuronal
308 morphology (Figure 4A), exemplarily shown for pyramidal cell layer of hippocampal CA1 region. In
309 contrast to NeuN-positive neurons, FITC-albumin-positive cells of neuronal morphology exhibited
310 only limited spatial overlap with endothelial basement membranes visualized by laminin
311 immunolabeling (Figure 4A’’). ~~It was described before that neurons can lose NeuN immunoreactivity~~
312 ~~despite preservation of nuclear membrane integrity after an ischemic brain insult (Ünal-Cevik et al.,~~
313 ~~2004). Ünal-Cevik and colleagues suggest that this loss of NeuN antigenicity might be caused by~~
314 ~~severe insult-induced metabolic perturbations of neurons, or by depletion or alteration of the~~
315 ~~antigen. Therefore, the colocalization of FITC-albumin with NeuN-negative cells of neuronal~~
316 ~~morphology, as described here, indicates FITC-albumin uptake by damaged, but morphologically~~
317 ~~integer neurons. This assumption is supported by data on extravasated albumin-bound Evans Blue~~
318 ~~after SE often in Fluoro-Jade B-positive, i.e. dying, neurons (van Vliet et al., 2007).~~

319 Spatial relationships between FITC-albumin and vascular markers combined with GFAP-expressing
320 astroglia are shown in the hippocampal pyramidal cell layer at lower magnification (Fig. 5A-A’’’) and
321 higher magnified (Fig. 5B-B’’’). FITC-albumin was again predominantly found in pyramidal cells, and

eNeuro Accepted Manuscript

322 to a lower extent in close vicinity to laminin-positive vascular structures (Fig. 5A), which becomes
323 more obvious in the merged staining patterns (arrow in Fig. 5A'''). In parallel, GFAP-immunopositive
324 structures (Fig. 5A'',B'') appeared separated in the overlays of staining patterns, which reveal
325 astrocytic endfeet contacting endothelial cells stained with biotinylated STL (arrow in Fig. 5B''').
326 Thalamic FITC-albumin apparently within cells (Fig. 6A) was additionally counterstained by collagen
327 IV-immunolabeling of basal membranes (Fig. 6A') and biotinylated STL detecting endothelial cells
328 (Fig. 6A''). The even distribution of STL-stained vessels contrasted with the local upregulation of
329 collagen IV expression. The overlay of staining patterns (Fig. 6A''') revealed that FITC-albumin-
330 positive areas concomitantly displayed up-regulated vascular collagen IV-immunoreactivity which
331 was frequently allocated with STL-binding sites also in thinned vessels.

332 Next, FITC-albumin and STL staining were combined with the immunodetection of AQP4 known as
333 marker for astrocytic endfeet. This triple staining is exemplarily shown in the thalamus at lower
334 magnification (Fig. 7A-A''') and higher magnified (Fig. 7B-B'''). SE-affected regions as indicated by
335 intracellular FITC-albumin (Fig. 7A,B) were largely devoid of immunosignals for AQP4 (asterisks in Fig.
336 7A',B') whereas adjacent tissue within the affected areas displayed much higher levels of vessel-
337 associated AQP4. In parallel, STL staining in the affected regions was either diminished (Fig. 7A'',
338 arrow) or appeared unaltered (Fig. 7B'',B''').

339 To analyze the spatial relationships between astroglial markers as well as between astrocytes and
340 FITC-albumin deposition, the immunolabeling of AQP4 was combined with the detection of GFAP
341 (Fig. 8A-A''') or S100β (Fig. 8B-B''') in SE-affected thalamic tissue containing FITC-albumin-filled cells.
342 FITC-albumin (Fig. 8A) was observed in regions lacking apparent AQP4-immunoreactivity (Fig. 8A')
343 and with weakened GFAP-immunodecoration (Fig. 8A''). Merged staining patterns (Fig. 8A''')
344 indicated a nearly complementary occurrence of FITC-albumin and AQP4 expression together with
345 remnants of mostly punctate GFAP-immunoreactive structures. Subsequently, FITC-albumin-positive
346 areas (Fig. 8B) were counterstained with anti-S100β (Fig. 8B') which predominantly reveals astroglial
347 somata with numerous processes, whereas the immunodetection of GFAP with Cy5 (Fig. 8B'', color-

eNeuro Accepted Manuscript

348 coded in blue) visualizes astrocytic intermediate filaments. The merged staining patterns (Fig. 8B''')
349 clearly demonstrated numerous astrocytes co-expressing both astroglia-specific markers, but lacking
350 allocated FITC-albumin.

351 For the simultaneous detection of astroglia and microglia/ macrophages, FITC-albumin was
352 counterstained with GFAP and Iba which is exemplified for the thalamus (Fig. 9A-A'''). SE-induced
353 leakage of the BBB again led to extravasation of FITC-albumin followed by its internalization by
354 neuron-like cells (Fig. 9A). Numerous Iba-immunopositive ameboid microglial cells were seen in the
355 same tissue (Fig. 9A') and were intermingled by active, proliferating astrocytes (Fig. 9A''). The overlay
356 of staining patterns (Fig. 9A''') only rarely indicated FITC-albumin-filled glial cells (Fig. 9A'''). Cy3-
357 immunodetection of Iba (Fig. 9B') was combined with the Cy5-staining of STL-binding sites which
358 were found in vessels as well as in ameboid perivascular microglia/macrophages (Fig. 9B''). A
359 majority of perivascular Iba-positive activated microglia displayed in the overlay of staining patterns
360 (Fig. 9B''') both lectin- and immunohistochemical labeling. FITC-albumin was occasionally also found
361 in Iba-positive microglia (arrowhead).

362 For specifying immune cells exemplified in the thalamus 48 h after SE, Iba was counterstained either
363 with anti-CD45c in activated microglia (Fig. 10A-A''') or with anti-CD8b in T lymphocytes (Fig. 10B-
364 B'''). FITC-albumin-filled cells (Fig. 10A) were observed in a clearly delineated zone with reduced Cy3-
365 immunolabeling of CD45c (Fig. 10A'), while Iba-immunoreactivity (Fig. 10A'') was found in ameboid
366 immune cells accumulating close to FITC-albumin-positive cells. Merged staining patterns (Fig. 10A''')
367 elucidated several cells co-expressing both microglial markers (arrow in Fig. 10A'''). At higher
368 magnification, FITC-albumin (Fig. 10B) was occasionally found in immune cells expressing CD8b (Fig.
369 10B') as well as Iba (Fig. 10B'') which is exemplified in the overlay (Fig. 10B''') by the arrow-marked
370 cell.

371 Table 2 provides a survey of the results gained by analysis of fluorescence staining. In brain sections
372 from control rats, neither extra- nor intracellular FITC-albumin was observed. Further, none of the

eNeuro Accepted Manuscript

373 alterations in immunosignals or abnormal staining patterns described above were seen in sections
374 from control rats which underwent the identical staining procedures (not shown).
375

376 **Discussion**

377 SE and prolonged febrile seizures represent clear risk factors for developing temporal lobe epilepsy
378 which is strongly supported by data from human and animal studies (French et al., 1993; Mathern et
379 al., 1995; Scott et al., 2003; Patterson et al., 2014), and BBB leakage is proposed to represent a
380 crucial event contributing to epileptogenesis (Marchi et al., 2007b; Friedman et al., 2009). Purpose of
381 this study was to provide comprehensive data on the spatiotemporal evolution of SE-induced BBB
382 leakage *in vivo* by translational MR imaging and *ex vivo* by complementary immunohistochemical
383 analyses characterizing the response of NVU components to the epileptogenic brain insult. Our data
384 provide important information for therapeutic intervention after epileptogenic brain insults and
385 suggest that a very prompt BBB-stabilizing intervention will be necessary to prevent distinct albumin
386 extravasation and subsequent pro-epileptogenic consequences following SE. The main findings are:
387 (i) SE-induced BBB leakage peaks between 1 and 2 days post SE affecting main epileptogenesis-
388 associated brain regions, and rapidly declines thereafter; (ii) increase in T2-weighted MRI mainly
389 follows the time course of contrast agent extravasation; (iii) at the time of maximum BBB leakage,
390 extravasated albumin colocalizes with the perivascular basement membranes, neurons, and brain
391 immune cells, but not with astrocytes; (iv) albumin-positive areas are characterized by reduced
392 immunoreactivity for astroglial markers (GFAP, AQP4), as well as endothelial STL-binding sites,
393 whereas collagen IV, a marker of perivascular basement membranes, is elevated.

394 Uncovering the time course of BBB leakage is of particular relevance for timing therapeutic
395 intervention during epileptogenesis. Although the temporal evolution of increased BBB permeability
396 was lately determined for another post-SE model of epileptogenesis (van Vliet et al., 2016),
397 respective data for the pilocarpine model, which is often applied to examine therapeutic intervention

eNeuro Accepted Manuscript

398 during epileptogenesis (Löscher, 2012), were not available so far. Here, we applied a translational
399 MRI-based imaging method, which we recently identified to be the method of choice for detection
400 and quantification of BBB leakage (Breuer et al., 2016). The leakage displayed its maximum about
401 two days after SE and clearly declined on day 4 suggesting a partial recovery of BBB integrity in
402 formerly affected brain regions like hippocampus and thalamus (Fig. 1). The persistently increased
403 BBB permeability in the piriform cortex at day 10 might indeed be indicative of continuous
404 epileptogenesis in this animal model. Comparable results from other post-SE models support this
405 idea. After electrically-induced SE, van Vliet et al. (2007) found increased albumin extravasation,
406 histologically assessed by analyses of fluorescein signals, still in the latent and, to a minor extent, also
407 in the chronic epilepsy phase in several epileptogenesis-associated brain regions including the
408 piriform cortex. The same group reported persistent leakage of contrast agent at 3 and 6 weeks post
409 kainate-induced SE as assessed by T1-weighted MRI in the amygdala/piriform cortex (van Vliet et al.,
410 2016). After paraoxon-induced SE, Bar-Klein et al. (2017) observed BBB leakage in the piriform
411 network at 2 days and 1 month, but not at 1 week, post SE in rats identified as epileptic later on,
412 nonetheless suggesting a persistent affection of this region after SE. Interestingly, van Vliet et al.
413 (2016) found a correlation between BBB leakage in the piriform cortex and seizure frequency in the
414 chronic phase, and Bar-Klein et al. (2017) identified BBB leakage in the piriform network as predictive
415 marker for epilepsy development underlining the importance of investigating changes accompanying
416 albumin extravasation on a cellular level.

417 Additionally, we evaluated T2-weighted MRI to spatio-temporally assess SE-induced brain edema and
418 inflammation, as T2-weighted MRI was suggested also as an indicator of active inflammation
419 (Michoux et al., 2015; Peixoto-Santos et al., 2017). T2-signal increase was found to a lesser extent
420 than T1-signal increase, but with a similar spatiotemporal profile (Fig. 1), suggesting cerebral edema
421 to appear predominantly early after SE and to resolve soon thereafter. Our findings correspond to
422 those of previous pre-clinical studies by Roch et al. (2002), Choy et al. (2010) and Duffy et al. (2014)
423 who detected peaks of T2 intensity around 2 to 4 days following pilocarpine-induced SE. Importantly,

eNeuro Accepted Manuscript

424 our data are also in line with clinical data on hippocampal edema to occur within 48 h after SE in
425 human subjects (VanLandingham et al., 1998; Scott et al., 2002). In a recent study, we longitudinally
426 assessed the time course of microglia activation after pilocarpine-induced SE by [^{11}C]PK11195
427 positron emission tomography (Brackhan et al., 2016). We found inflammation peaking between 1
428 and 2 weeks post SE, i.e. distinctly later than T2-signal increase observed in the present study,
429 suggesting that T2-weighted MRI does not only reflect microglia activation but also other aspects of
430 post-SE neuroinflammation. As the T2 MRI signal is strongly dependent on stationary water
431 concentration, brain water homeostasis might be impaired by altered astrocytic AQP4 function. A
432 recent study in human TLE patients indeed demonstrated that increased T2 relaxation time
433 correlates with astrogliosis, microgliosis and chondroitin sulfate proteoglycan expression (Peixoto-
434 Santos et al., 2017). In the same patients, expression of AQP4 in astrocytic endfeet was distinctly
435 reduced.

436 To substantiate our analysis, we performed additional histological assessment of FITC-albumin
437 extravasation. Importantly, extravasation patterns analyzed *ex vivo* were generally congruent with *in*
438 *vivo* MRI findings (Fig. 1 and 2). Our results corroborate peak albumin extravasation between 24 and
439 48 h after SE. While converting the albumin signal into a light-microscopically visible adduct
440 (Michalski et al., 2010) provides quantitative values even at electron microscopic level (Krueger et al.,
441 2015), the score-based analysis gives similar results and allows to differentiate between extra- and
442 intracellular appearance of green fluorescence. Detection of intracellular FITC-albumin at 5 h post SE
443 demonstrates that cells of neuron-like shape are pathologically affected at this time point to allow
444 albumin uptake. Here, we used intravenous injection of FITC-albumin with the intention to reveal the
445 actual extent and localization of extravasated albumin at the chosen time points after SE. In contrast,
446 staining of endogenous albumin at the respective time points would have resulted in information
447 about the cumulative amount of albumin extravasated during the whole time span between SE and
448 time of sacrifice. There is no evidence that dyes of low molecular weight (as compared to the MW of
449 albumin), covalently bound or not, alter the crossing properties of albumin at the BBB. Furthermore,

eNeuro Accepted Manuscript

450 crossing of endogenous albumin will only be relevantly influenced by exogenous FITC-albumin when
451 given in high amounts. Notably, the administered amount of FITC-albumin (100 mg/kg) relates to less
452 than 5% of the average endogenous albumin blood concentration in adult Sprague-Dawley rats (3
453 g/dl, Zaias et al., 2009), resulting, if at all, in a slight underestimation of the amount of extravasated
454 albumin.

455 Histological examinations were performed to evaluate consequences of albumin extravasation for
456 the NVU in further detail (Table 2). Areas with albumin extravasation and uptake in neuron-like cells
457 also showed loss of NeuN-immunoreactivity and colocalization with the vascular basement
458 membrane marker laminin (Fig. 3). It was described before that neurons can lose NeuN
459 immunoreactivity despite preservation of nuclear membrane integrity after an ischemic brain insult
460 (Ünal-Cevik et al., 2004). Ünal-Cevik and colleagues suggest that this loss of NeuN antigenicity might
461 be caused by severe insult-induced metabolic perturbations of neurons, or by depletion or alteration
462 of the antigen. Therefore, the colocalization of FITC-albumin with NeuN-negative cells of neuronal
463 morphology, as described here, indicates FITC-albumin uptake by damaged, but morphologically
464 integer neurons. This assumption is supported by data on extravasated albumin-bound Evans'-blue
465 after SE often in Fluoro-Jade B-positive, i.e. dying, neurons (van Vliet et al., 2007). This is also in line
466 with the distinct neurodegeneration found on days one and two after SE in Nissl-stained temporal
467 lobe subregions (Fig. 2). Unfortunately, Fluoro-Jade staining representing the best evaluated marker
468 of dying neurons could not be evaluated here as its light emission profile and that of fluorescein are
469 considerably interfering. In concordance with our data, neurons were reported to be the only or
470 major cell type containing albumin following acute seizures or SE, i.e. in an affected brain (Marchi et
471 al., 2007a; van Vliet et al., 2007, Frigerio et al., 2012). Accordingly, neuronal uptake was frequently
472 observed in regions of Evans Blue extravasation in the porcine hippocampus following osmotic BBB
473 impairment and adherent acute seizures (Marchi et al., 2007b). However, *in vitro* exposure of naïve
474 rat cortical brain slices to FITC-albumin or prolonged (72 h) infusion of albumin into the lateral
475 ventricle of naïve mice did not result in colocalization of albumin with neurons (Ivens et al., 2007;

eNeuro Accepted Manuscript

476 Weissberg et al., 2015). These conflicting findings suggest that albumin behaves different in the
477 seizing *versus* the naïve brain, and that albumin uptake into neurons might be favored by an
478 impaired environment. This assumption is also supported by Michalak et al. (2012) who tracked the
479 uptake of extravasated IgG into neurons in chronic TLE patients and rats during epileptogenesis.

480 Assessment of albumin colocalization with a variety of further cellular markers exposed spatial
481 overlap of albumin also with microglia and CD8b-positive T cells (Figs. 3-9). Surprisingly and despite
482 the use of three markers labeling different astrocytic compartments, i.e. intermediate filaments
483 (GFAP), predominantly somata (S100ß), and endfeet (AQP4), astroglia were devoid of detectable
484 FITC-albumin in the present study. This is in contrast to the reported selective transport of albumin
485 into astrocytes in vitro in cortical brain slices or cultured astrocytes (Ivens et al., 2007; Bar-Klein et
486 al., 2014), but in general accordance with observations after electrically-induced SE (van Vliet et al.,
487 2007) and after acute seizures (Marchi et al., 2007a). Furthermore, we show that in FITC-albumin-
488 positive areas after SE, staining intensity of astrocytic markers was reduced (GFAP) or lacking (AQP4),
489 indicating a severe disturbance of the endothelial-neuronal coupling mediated by astrocytes. In
490 earlier studies, we and others observed significantly increased activation of astroglia at light-
491 microscopic level in epileptogenesis-associated brain regions after pilocarpine-induced SE (cf. Zhang
492 et al., 2015, Brackhan et al., 2016). Applying laser-scanning microscopy, we here observed the
493 reduced immunoreactivities for GFAP and AQP4 in albumin-positive areas in proximity to the blood
494 vessels of the NVU, i.e. this finding holds mainly for the astrocyte compartments contributing to BBB
495 constitution. This may be due to a locally higher albumin concentration or more distinct alterations in
496 ion concentrations close to leaky brain capillaries. Reduced AQP4 staining was also described by Lee
497 et al. (2012a) in mice during epileptogenesis after kainate-induced SE. Importantly, partial loss of
498 perivascular AQP4 was also found in hippocampi of epilepsy patients (Eid et al., 2005). Very recently,
499 Peixoto-Santos (2017) reported decreased AQP4 polarity, i.e. loss of AQP4 expression in astrocyte
500 proximal processes and end feet close to brain blood vessels of TLE patients. Additionally, our
501 observations suggest that at sites of albumin leakage components of STL-stained endothelial cells are

eNeuro Accepted Manuscript

502 less present than in areas without visible FITC-albumin. In combination with the reduced AQP4 and
503 increased collagen IV-immunoreactivity, these alterations point to a distinct adaptive reorganization
504 process of the NVU vasculature taking place within 48 h after SE. The obvious impairment of
505 astrocytes (reduced GFAP and AQP4) might entail disordered or dying neurons, e.g. by reduced
506 glutamate uptake from the extracellular space resulting in neurotoxic concentrations, or by impaired
507 astrocytic energy supply for neurons, an assumption supported by *in vivo* PET imaging studies
508 demonstrating cerebral glucose hypometabolism shortly after SE (Goffin et al., 2009; Guo et al.,
509 2009; Jupp et al., 2012; Lee et al., 2012b; Zhang et al., 2015).

510 As collagen IV is a stabilizing constituent in the vascular architecture of the NVU and part of the
511 immunological BBB (Dyrna et al., 2013), the observed increase in collagen IV-immunoreactivity at
512 sides of BBB leakage could represent the beginning of local repair processes to re-establish BBB
513 integrity. Interestingly, increased collagen IV expression was also observed following other brain
514 insults leading to NVU/BBB injury like experimental stroke (Hawkes et al., 2013). Moreover,
515 colocalization of FITC-albumin with brain immune cell markers (Iba, CD45c for activated microglia)
516 and CD8b (for T cells) did not reveal any obvious cellular preference, suggesting involvement of the
517 entire brain immune system in epileptogenesis-associated remodeling of the NVU.

518 In conclusion, we provide a detailed *in vivo* and *ex vivo* analysis of the spatiotemporal course of BBB
519 leakage and associated NVU alterations focusing on the early time period post SE in a widely used rat
520 model of epileptogenesis. Our data suggest that BBB damage is an important factor triggering
521 epileptogenesis-associated changes and arises very soon after SE. Subsequent degenerative events at
522 the level of the NVU, including degeneration of brain vessels, astrocytes and neurons, seem to
523 outweigh reconstructive processes. The seizing brain with leaky BBB seems to promote
524 predominantly neuronal albumin uptake, an observation requiring further investigation to define its
525 role in epilepsy development. Taken together, our data support the suggestion that early BBB-
526 restoring treatment, such as isoflurane (Bar-Klein et al., 2016), glucocorticoids (Marchi et al., 2012) or
527 levetiracetam (Itoh et al., 2016), might be one reasonable component of rational therapeutic

528 intervention to ameliorate the development of temporal lobe epilepsy and other detrimental

529 sequelae of SE.

530

eNeuro Accepted Manuscript

eNeuro Accepted Manuscript

531 **References**

532 Bankstahl M, Bankstahl JP, Löscher W (2012) Inter-individual variation in the anticonvulsant effect of
533 phenobarbital in the pilocarpine rat model of temporal lobe epilepsy. Exp Neurol 234:70-84.
534 Bar-Klein G, Lublinsky S, Kamintsky L, Noyman I, Veksler R, Dalipaj H, Senatorov VV Jr, Swissa E,
535 Rosenbach D, Elazary N, Milikovsky DZ, Milk N, Kassirer M, Rosman Y, Serlin Y, Eisenkraft A,
536 Chassidim Y, Parmet Y, Kaufer D, Friedman A (2017) Imaging blood-brain barrier dysfunction
537 as a biomarker for epileptogenesis. Brain 140:1692-1705.
538 Bar-Klein G, Klee R, Brandt C, Bankstahl M, Bascunana P, Töllner K, Dalipaj H, Bankstahl JP, Friedman
539 A, Löscher W (2016) Isoflurane prevents acquired epilepsy in rat models of temporal lobe
540 epilepsy. Ann Neurol 80:896-908.
541 Bar-Klein G, Cacheaux LP, Kamintsky L, Prager O, Weissberg I, Schoknecht K, Cheng P, Kim SY, Wood
542 L, Heinemann U, Kaufer D, Friedman A (2014) Losartan prevents acquired epilepsy via TGF-
543 beta signaling suppression. Ann Neurol 75:864-875.
544 Brackhan M, Bascunana P, Postema JM, Ross TL, Bengel FM, Bankstahl M, Bankstahl JP (2016) Serial
545 quantitative TSPO-targeted PET reveals peak microglial activation up to two weeks after an
546 epileptogenic brain insult. J Nucl Med 57:1302-1308.
547 Brandt C, Töllner K, Klee R, Bröer S, Löscher W (2015) Effective termination of status epilepticus by
548 rational polypharmacy in the lithium-pilocarpine model in rats: Window of opportunity to
549 prevent epilepsy and prediction of epilepsy by biomarkers. Neurobiol Dis 75:78-90.
550 Breuer H, Meier M, Schneefeld S, Härtig W, Wittneben A, Märkel M, Ross TL, Bengel FM, Bankstahl
551 M, Bankstahl JP (2017) Multimodality imaging of blood-brain barrier impairment during
552 epileptogenesis. J Cereb Blood Flow Metab 37:2049-2061.
553 Bröer S, Löscher W (2015) Novel combinations of phenotypic biomarkers predict development of
554 epilepsy in the lithium-pilocarpine model of temporal lobe epilepsy in rats. Epilepsy Behav
555 53:98-107.

eNeuro Accepted Manuscript

556 Choy M, Cheung KK, Thomas DL, Gadian DG, Lythgoe MF, Scott RC (2010) Quantitative MRI predicts
557 status epilepticus-induced hippocampal injury in the lithium-pilocarpine rat model. Epilepsy
558 Res 88:221-230.
559 Duffy BA, Chun KP, Ma D, Lythgoe MF, Scott RC (2014) Dexamethasone exacerbates cerebral edema
560 and brain injury following lithium-pilocarpine induced status epilepticus. Neurobiol Dis
561 63:229-236.
562 Dyrna F, Hanske S, Krueger M, Bechmann I (2013) The blood-brain barrier. J Neuroimmune
563 Pharmacol 8:763-773.
564 Eid T, Lee TS, Thomas MJ, Amiry-Moghaddam M, Bjornsen LP, Spencer DD, Agre P, Ottersen OP, de
565 Lanerolle NC (2005) Loss of perivascular aquaporin 4 may underlie deficient water and K+
566 homeostasis in the human epileptogenic hippocampus. Proc Natl Acad Sci U S A 102:1193-
567 1198.
568 French JA, Williamson PD, Thadani VM, Darcey TM, Mattson RH, Spencer SS, Spencer DD (1993)
569 Characteristics of medial temporal lobe epilepsy: I. Results of history and physical
570 examination. Ann Neurol 34:774-780.
571 Friedman A, Heinemann U (2012) Role of Blood-Brain Barrier Dysfunction in Epileptogenesis. In:
572 Jasper's Basic Mechanisms of the Epilepsies (Noebels JL, Avoli M, Rogawski MA, Olsen RW,
573 Delgado-Escueta AV, eds). Bethesda (MD): National Center for Biotechnology Information
574 (US).
575 Friedman A, Kaufer D, Heinemann U (2009) Blood-brain barrier breakdown-inducing astrocytic
576 transformation: novel targets for the prevention of epilepsy. Epilepsy Res 85:142-149.
577 Frigerio F, Frasca A, Weissberg I, Parrella S, Friedman A, Vezzani A, Noe, FM (2012) Long-lasting pro-
578 ictogenic effects induced in vivo by rat brain exposure to serum albumin in the absence of
579 concomitant pathology. Epilepsia. 53:1887-1897.
580 Goffin K, Van Paesschen W, Dupont P, Van Laere K (2009) Longitudinal microPET imaging of brain
581 glucose metabolism in rat lithium-pilocarpine model of epilepsy. Exp Neurol 217:205-209.

eNeuro Accepted Manuscript

582 Guo Y, Gao F, Wang S, Ding Y, Zhang H, Wang J, Ding MP (2009) In vivo mapping of temporospatial
583 changes in glucose utilization in rat brain during epileptogenesis: an 18F-fluorodeoxyglucose-
584 small animal positron emission tomography study. Neuroscience 162:972-979.
585 Hawkes CA, Michalski D, Anders R, Nissel S, Grosche J, Bechmann I, Carare RO, Härtig W (2013)
586 Stroke-induced opposite and age-dependent changes of vessel-associated markers in co-
587 morbid transgenic mice with Alzheimer-like alterations. Exp Neurol 250:270-281.
588 Itoh K, Ishihara Y, Komori R, Nochi H, Taniguchi R, Chiba Y, Ueno M, Takata-Tsuji F, Dohgu S, Kataoka
589 Y (2016) Levetiracetam treatment influences blood-brain barrier failure associated with
590 angiogenesis and inflammatory responses in the acute phase of epileptogenesis in post-
591 status epilepticus mice. Brain Res 1652:1-13.
592 Ivens S, Kaufer D, Flores LP, Bechmann I, Zumsteg D, Tomkins O, Seiffert E, Heinemann U, Friedman A
593 (2007) TGF-beta receptor-mediated albumin uptake into astrocytes is involved in neocortical
594 epileptogenesis. Brain 130:535-547.
595 Janigro D (2012) Are you in or out? Leukocyte, ion, and neurotransmitter permeability across the
596 epileptic blood-brain barrier. Epilepsia 53 Suppl 1:26-34.
597 Jupp B, Williams J, Binns D, Hicks RJ, Cardamone L, Jones N, Rees S, O'Brien TJ (2012)
598 Hypometabolism precedes limbic atrophy and spontaneous recurrent seizures in a rat model
599 of TLE. Epilepsia 53:1233-1244.
600 Krueger M, Bechmann I, Immig K, Reichenbach A, Härtig W, Michalski D (2015) Blood-brain barrier
601 breakdown involves four distinct stages of vascular damage in various models of
602 experimental focal cerebral ischemia. J Cereb Blood Flow Metab 35:292-303.
603 Lee DJ, Hsu MS, Seldin MM, Arellano JL, Binder DK (2012a) Decreased expression of the glial water
604 channel aquaporin-4 in the intrahippocampal kainic acid model of epileptogenesis. Exp
605 Neurol 235:246-255

eNeuro Accepted Manuscript

606 Lee EM, Park GY, Im KC, Kim ST, Woo CW, Chung JH, Kim KS, Kim JS, Shon YM, Kim YI, Kang JK (2012b)
607 Changes in glucose metabolism and metabolites during the epileptogenic process in the
608 lithium-pilocarpine model of epilepsy. Epilepsia 53:860-869.
609 Löscher W (2012) Strategies for antiepileptogenesis: Antiepileptic drugs versus novel approaches
610 evaluated in post-status epilepticus models of temporal lobe epilepsy. In: Jasper's Basic
611 Mechanisms of the Epilepsies (Noebels JL, Avoli M, Rogawski MA, Olsen RW, Delgado-
612 Escueta AV, eds). Bethesda MD.
613 Marchi N, Granata T, Ghosh C, Janigro D (2012) Blood-brain barrier dysfunction and epilepsy:
614 pathophysiologic role and therapeutic approaches. Epilepsia 53:1877-1886.
615 Marchi N, Oby E, Batra A, Uva L, De Curtis M, Hernandez N, Van Boxel-Dezaire A, Najm I, Janigro D
616 (2007a) In vivo and in vitro effects of pilocarpine: relevance to ictogenesis. Epilepsia 48:1934-
617 1946.
618 Marchi N, Angelov L, Masaryk T, Fazio V, Granata T, Hernandez N, Hallene K, Diglaw T, Franic L, Najm
619 I, Janigro D (2007b) Seizure-promoting effect of blood-brain barrier disruption. Epilepsia
620 48:732-742.
621 Marcon J, Gagliardi B, Balosso S, Maroso M, Noe F, Morin M, Lerner-Natoli M, Vezzani A, Ravizza T
622 (2009) Age-dependent vascular changes induced by status epilepticus in rat forebrain:
623 implications for epileptogenesis. Neurobiol Dis 34:121-132.
624 Mathern GW, Pretorius JK, Babb TL (1995) Influence of the type of initial precipitating injury and at
625 what age it occurs on course and outcome in patients with temporal lobe seizures. J
626 Neurosurg 82:220-227.
627 Michalak Z, Sano T, Engel T, Miller-Delaney SF, Lerner-Natoli M, Henshall DC (2013) Spatio-temporally
628 restricted blood-brain barrier disruption after intra-amygdala kainic acid-induced status
629 epilepticus in mice. Epilepsy Res 103:167-179.

eNeuro Accepted Manuscript

630 Michalak Z, Lebrun A, Di Miceli M, Rousset MC, Crespel A, Coubes P, Henshall DC, Lerner-Natoli M,
631 Rigau V (2012) IgG leakage may contribute to neuronal dysfunction in drug-refractory
632 epilepsies with blood-brain barrier disruption. J Neuropathol Exp Neurol 71:826-838.
633 Michalski D, Grosche J, Pelz J, Schneider D, Weise C, Bauer U, Kacza J, Gärtner U, Hobohm C, Härtig W
634 (2010) A novel quantification of blood-brain barrier damage and histochemical typing after
635 embolic stroke in rats. Brain Res 1359:186-200.
636 Michoux N, Guillet A, Rommel D, Mazzamuto G, Sindic C, Duprez T (2015) Texture Analysis of T2-
637 Weighted MR Images to Assess Acute Inflammation in Brain MS Lesions. PLoS One
638 10:e0145497.
639 Patterson KP, Baram TZ, Shinnar S (2014) Origins of temporal lobe epilepsy: febrile seizures and
640 febrile status epilepticus. Neurotherapeutics 11:242-250.
641 Paxinos G, Watson C (2007) The rat brain in stereotaxic coordinates, 6th Edition. Amsterdam:
642 Academic Press.
643 Peixoto-Santos JE, Kandratavicius L, Velasco TR, Assirati JA, Carlotti CG, Scandiuzzi RC, Salmon CE,
644 Santos AC, Leite JP (2017) Individual hippocampal subfield assessment indicates that matrix
645 macromolecules and gliosis are key elements for the increased T2 relaxation time seen in
646 temporal lobe epilepsy. Epilepsia 58:149-159.
647 Pitkänen A, Immonen R (2014) Epilepsy related to traumatic brain injury. Neurotherapeutics 11:286-
648 296.
649 Pitkänen A, Löscher W, Vezzani A, Becker AJ, Simonato M, Lukasiuk K, Gröhn O, Bankstahl JP,
650 Friedman A, Aronica E, Gorter JA, Ravizza T, Sisodiya SM, Kokaia M, Beck H (2016) Advances
651 in the development of biomarkers for epilepsy. Lancet Neurol 15:843-856.
652 Polascheck N, Bankstahl M, Löscher W (2010) The COX-2 inhibitor parecoxib is neuroprotective but
653 not antiepileptogenic in the pilocarpine model of temporal lobe epilepsy. Exp Neurol
654 224:219-233.

eNeuro Accepted Manuscript

655 Roch C, Leroy C, Nehlig A, Namer IJ (2002) Magnetic resonance imaging in the study of the lithium-
656 pilocarpine model of temporal lobe epilepsy in adult rats. Epilepsia 43:325-335.
657 Schmidt D, Sillanpää M (2016) Prevention of Epilepsy: Issues and Innovations. Curr Neurol Neurosci
658 Rep 16:95.
659 Schwarz AJ, Danckaert A, Reese T, Gozzi A, Paxinos G, Watson C, Merlo-Pich EV, Bifone A (2006) A
660 stereotaxic MRI template set for the rat brain with tissue class distribution maps and co-
661 registered anatomical atlas: application to pharmacological MRI. Neuroimage 32:538-550.
662 Scott RC, King MD, Gadian DG, Neville BG, Connelly A (2003) Hippocampal abnormalities after
663 prolonged febrile convulsion: a longitudinal MRI study. Brain 126:2551-2557.
664 Scott RC, Gadian DG, King MD, Chong WK, Cox TC, Neville BG, Connelly A (2002) Magnetic resonance
665 imaging findings within 5 days of status epilepticus in childhood. Brain 125:1951-1959.
666 Seiffert E, Dreier JP, Ivens S, Bechmann I, Tomkins O, Heinemann U, Friedman A (2004) Lasting blood-
667 brain barrier disruption induces epileptic focus in the rat somatosensory cortex. J Neurosci
668 24:7829-7836.
669 Tang FR, Loke WK, Ling EA (2011) Comparison of status epilepticus models induced by pilocarpine
670 and nerve agents - a systematic review of the underlying aetiology and adopted therapeutic
671 approaches. Curr Med Chem 18:886-899.
672 Ünal-Cevik I, Kilinc M, Gursoy-Özdemir Y, Gurer G, Dalkara T (2004) Loss of NeuN immunoreactivity
673 after cerebral ischemia does not indicate neuronal cell loss: a cautionary note. Brain Res
674 1015:169-174.
675 van Vliet EA, da Costa Araujo S, Redeker S, van Schaik R, Aronica E, Gorter JA (2007) Blood-brain
676 barrier leakage may lead to progression of temporal lobe epilepsy. Brain 130:521-534.
677 van Vliet EA, Otte WM, Wadman WJ, Aronica E, Kooij G, de Vries HE, Dijkhuizen RM, Gorter JA (2016)
678 Blood-brain barrier leakage after status epilepticus in rapamycin-treated rats I: Magnetic
679 resonance imaging. Epilepsia 57:59-69.

eNeuro Accepted Manuscript

680 VanLandingham KE, Heinz ER, Cavazos JE, Lewis DV (1998) Magnetic resonance imaging evidence of
681 hippocampal injury after prolonged focal febrile convulsions. Ann Neurol 43:413-426.
682 Walker LE, Janigro D, Heinemann U, Riikonen R, Bernard C, Patel M (2016) WONOEP appraisal:
683 Molecular and cellular biomarkers for epilepsy. Epilepsia 57:1354-1362.
684 Weissberg I, Wood L, Kamintsky L, Vazquez O, Milikovsky DZ, Alexander A, Oppenheim H, Ardizzone
685 C, Becker A, Frigerio F, Vezzani A, Buckwalter MS, Huguenard JR, Friedman A, Kaufer D (2015)
686 Albumin induces excitatory synaptogenesis through astrocytic TGF-beta/ALK5 signaling in a
687 model of acquired epilepsy following blood-brain barrier dysfunction. Neurobiol Dis 78:115-
688 125.
689 Zaias J, Mineau M, Cray C, Yoon D, Altman NH (2009) Reference values for serum proteins of
690 common laboratory rodent strains. J Am Assoc Lab Anim Sci. 48:387-390.
691 Zhang L, Guo Y, Hu H, Wang J, Liu Z, Gao F (2015) FDG-PET and NeuN-GFAP immunohistochemistry of
692 hippocampus at different phases of the pilocarpine model of temporal lobe epilepsy. Int J
693 Med Sci 12:288-294.

694

eNeuro Accepted Manuscript

695 **Figure legends**

696 **Figure 1**

697 Spatiotemporal course of blood-brain barrier (BBB) impairment and cerebral edema following status
698 epilepticus (SE) as assessed *in vivo* by 7T MRI. (A) Exemplary contrast-enhanced T1-weighted coronal
699 brain images in identical grey scale displaying region-dependent severity of blood-brain barrier (BBB)
700 leakage during epileptogenesis at 5 h, 48 h, 4 days and 10 days post status epilepticus (SE). (B)
701 Quantified T1-modified driven equilibrium Fourier transform (MDEFT) values measured after infusion
702 of gadolinium-diethylenetriamine pentaacetic acid (Gd-DTPA) as surrogate marker for BBB leakage
703 prior to (n = 13), 5 h (n = 5), 48 h (n = 5), 4 days (n = 6) and 10 days (n = 5) post SE. (C) Exemplary T2-
704 weighted coronal brain images displaying region-dependent severity of cerebral edema during
705 epileptogenesis. (D) Quantified T2 multi-slice-multi-echo (MSME) values measured prior to (n = 13), 5
706 h (n = 4), 48 h (n = 5), 4 days (n = 6) and 10 days (n = 5) post SE. Data in (B) and (D) are normalized to
707 pons and illustrated as mean ± SEM. $^{*}p < 0.05$ *versus* baseline (B), one-way ANOVA, Dunnett's post-
708 hoc test.

709 **Figure 2**

710 Histological evaluation of albumin extravasation during early epileptogenesis. (A) Distribution of
711 FITC-labeled albumin (FITC-Alb) after its conversion into a light microscopically visible adduct with
712 anti-FITC-HRP and nickel-enhanced DAB in a representative section from a rat 48 h following status
713 epilepticus (SE). The extravasation marker indicating leakage of allocated BBB is predominantly
714 visible in the thalamus and the piriform cortex. Scale bar = 1 mm. (B) Quantification of DAB-positive
715 area relative to the total section area in control rats (n = 10), and rats at 5 h (n = 6), 24 h (n = 5), and
716 48 h (n = 16) following SE. $^{*}p<0.05$ compared to control, one-way ANOVA, Dunnett's multiple
717 comparison test. (C) Coronal Gd-DTPA-enhanced T1 MRI leakage map resulting from comparison
718 between baseline and 48 h post SE. Note the striking similarity of BBB leakage pattern in the ex-vivo
719 DAB-converted FITC-albumin slice (A) and *in vivo* contrast-enhanced MRI (C). Leakage t-map was

eNeuro Accepted Manuscript

720 calculated by SPM12 software (two-sample unpaired t-test, p<0.001, and a minimum cluster size of
721 100 voxels; scale bar displays t-values). (D) Exemplary whole brain sections and a higher magnified
722 image of the thalamus from two rats, predominantly showing extracellular distribution (left, 48 h
723 post SE) or intracellular uptake (right, 24 h post SE) of extravasated FITC-labeled albumin. (E) Semi-
724 quantitative analysis of extracellular FITC-labeled albumin in control rats (n = 10), and rats at 5 h (n =
725 6), 24 h (n = 5), and 48 h (n = 14) following SE. (F) Semi-quantitative analysis of intracellular FITC-
726 labeled albumin in control rats (n = 10), and rats at 5 h (n = 6), 24 h (n = 5), and 48 h (n = 14) following
727 SE. (E) and (F) show peak values of FITC-albumin presence at 24 h post SE. *p<0.05 compared to
728 control, Kruskal-Wallis ANOVA, Dunn's multiple comparison test. Data are illustrated as box-and-
729 whisker plots. Co, control, Pir./entorh., piriform/entorhinal.

730 **Figure 3**

731 Histological evaluation of neurodegeneration during early epileptogenesis. (A) Representative images
732 of Nissl-stained forebrain sections (-3.6 mm relative to bregma; left hemisphere; hippocampus,
733 piriform cortex/amygdala) of a control rat and rats 5, 24, and 48 h following status epilepticus (SE).
734 Scale bar = 500 µm. (B) Number of hilar neurons in control rats (n = 6), and rats at 5 h (n = 6), 24 h (n
735 = 5), and 48 h (n = 4) following SE, revealing neurodegeneration only at 48 h post SE. (C) Semi-
736 quantitative analysis of neurodegeneration in hippocampal subregions, amygdala, as well as cortical
737 subregions in control rats (n = 6), and rats at 5 h (n = 6), 24 h (n = 5), and 48 h (n = 4) following SE.
738 *p<0.05 compared to control, (B) one-way ANOVA, Dunnett's multiple comparison test, (C) Kruskal-
739 Wallis ANOVA, Dunn's multiple comparison test. Data are illustrated as box-and-whisker plots. CA,
740 cornu ammonis. Co, control, Pir./entorh., piriform/entorhinal.

741 **Figure 4**

742 Concomitant detection of FITC-coupled albumin (FITC-Alb) (A) in the pyramidal layer of the
743 hippocampal CA1 region 48 h after SE shows predominantly intracellular FITC-Alb. Neuronal somata
744 are stained with biotinylated anti-NeuN and red fluorescent Cy3-streptavidin (A'), while vascular

eNeuro Accepted Manuscript

745 basement membranes are visualized with rabbit-anti-laminin and Cy5-donkey anti-rabbit IgG (A'',
746 immunosignals color-coded in blue). The overlay of staining patterns (A''') elucidates only rare
747 colocalization of FITC-Alb and NeuN-positive neurons. Scale bar = 50 µm.

748 **Figure 5**

749 Hippocampal pyramidal cell layer in the CA1 region with FITC-coupled albumin (FITC-Alb) (A,B) 48 h
750 following SE and (A') laminin-immunoreactivity in vascular basement membranes (Cy3, red) or (B')
751 endothelial binding sites for biotinylated *Solanum tuberosum* lectin (STL; endothelial cells, Cy3, red),
752 each combined with immunolabeling of astroglial GFAP (A'', B'', Cy5, color-coded in blue) at lower
753 magnification (A-A''') and higher magnified (B-B'''). Merged staining patterns (A''', B''') elucidate
754 FITC-Alb in close vicinity to laminin-immunopositive structures (arrow in A'''), but no obvious
755 colocalization of FITC-Alb and GFAP-positive astrocytes (A''', B'''). Scale bars: A'' (also valid for A, A') =
756 100 µm, A''' = 50 µm, B'' (also valid for B, B') = 50 µm, B''' = 25 µm.

757 **Figure 6**

758 Simultaneous demonstration of thalamic FITC-coupled albumin (FITC-Alb) 24 h following SE
759 combined with the detection of the vascular marker collagen IV and binding sites for *Solanum*
760 *tuberosum* lectin (STL). FITC-Alb (A) is seen in neuron-like cells in SE-affected regions, mainly marked
761 by apparently up-regulated collagen IV (Coll IV)-immunoreactivity (A', Cy3, red). Concomitant lectin-
762 histochemical staining with STL (A'', Cy5, color-coded in blue) reveals vessels which appear thinner
763 and of lower STL signal in tissue with detectable FITC-Alb. Vascular structures containing both Coll IV
764 and STL-binding sites appear purple in (A'''). Scale bar = 75 µm.

765 **Figure 7**

766 Concomitant visualization of thalamic FITC--coupled albumin (FITC-Alb) 24 h after SE with astroglial
767 aquaporin-4 (AQP4, astrocytic endfeet) and endothelial *Solanum tuberosum* lectin (STL) binding as
768 overview (A-A''') and at higher magnification (B-B'''). FITC-Alb is seen in numerous neuron-like cell
769 somata (A, B). AQP4 immunolabeling (A', B') is largely absent in FITC-Alb-positive tissue marked by

eNeuro Accepted Manuscript

770 asterisks in A’, but distinctly expressed in adjacent areas. STL staining in the same area appears
771 diminished (A’’, arrow). The overlay of staining patterns (A’’’, B’’’) elucidates allocated AQP4-
772 immunoreactive astrocytic endfeet and endothelial STL-binding sites appearing as purple vessels in
773 close vicinity to many FITC-Alb-filled cells. Scale bars: A’’ (also valid for A, A’) = 200 µm, A’’’ = 100 µm,
774 B’’ (also valid for B, B’) = 50 µm, B’’’ = 25 µm.

775 **Figure 8**

776 Detection of GFAP and cellular FITC-coupled albumin (FITC-Alb) in SE-affected thalamus 48 h after SE
777 onset combined with immunolabeling of aquaporin-4 (AQP4; A-A’’’) or of S100β (B-B’’’). FITC-Alb in
778 (A) is seen in region devoid of Cy3-staining for AQP4 (A’) and diminished GFAP-immunosignals (A’’).
779 The overlay of staining patterns (A’’’) reveals a nearly complementary occurrence of FITC-Alb and
780 AQP4 expression, but also shows remnants of mostly punctuate GFAP-immunoreactive structures. At
781 higher magnification, in another thalamic area from the same animal Cy3-counterstaining of S100β
782 (B’) predominantly reveals astroglial somata with numerous processes, whereas the
783 immunodetection of GFAP with Cy5 (B’’, color-coded in blue) visualizes astrocytic intermediate
784 filaments. The merge of staining patterns (B’’’) clearly demonstrates numerous astrocytes co-
785 expressing both astroglia-specific markers, but lacking allocated FITC-Alb. Scale bars: A’’ (also valid
786 for A, A’) = 100 µm, A’’’ = 50 µm, B’’ (also valid for B, B’) = 50 µm, B’’’ = 25 µm.

787 **Figure 9**

788 Demonstration of FITC-coupled albumin (FITC-Alb) and Iba-immunoreactive microglia/macrophages
789 combined with thalamic GFAP immunolabeling 48 h after SE onset (A-A’’’) and the detection of
790 hippocampal *Solanum tuberosum* lectin (STL)-binding sites 24 h after SE onset (endothelial cells, B-
791 B’’’). FITC-Alb in the thalamus is predominantly visible within neuron-like cells (A). The same region
792 contains Iba-immunopositive ameboid microglia which is even stronger labelled in adjacent tissue
793 with less FITC-Alb (A’). In parallel, proliferating astrocytes are revealed by GFAP-immunostaining (A’’).
794 The merge of staining patterns (A’’’) allows for the identification of single FITC-Alb-filled immune cells

795 displaying the mixed color yellow (arrow in A'''). Additionally, hippocampal FITC-Alb-positive cells are

796 allocated with Cy5-staining of STL-binding sites and Cy3-immunolabeling of Iba (arrowhead, B''').

797 Scale bars: A'', B'' (also valid for A, A', B, B') = 100 µm, A''', B''' = 50 µm.

798 **Figure 10**

799 Triple fluorescence labeling of FITC-coupled albumin (FITC-Alb) and Iba combined with the

800 immunodetection either of immune cells expressing CD45c (A-A''') or CD8b (B-B''') in thalamic

801 regions 48 h after SE. FITC-Alb-filled cells are here restricted to a clearly delineated zone (A), whereas

802 CD45c-immunodetection (A') visualizing the leukocyte common antigen is stronger in tissue devoid

803 visible FITC-Alb and Iba (A''), which is seen in more evenly distributed ameboid immune cells. The

804 overlay of staining patterns (A''') clearly shows several cells co-expressing both microglial markers

805 (exemplified by arrows in A'''), whereas all FITC-Alb-stained cells appear mono-labeled. At higher

806 magnification, one cell displays not only a cytoplasmic label with FITC-Alb (B), but also a small, round

807 compartment with a much stronger fluorescence signal. This cell and three other cells with similar

808 ameboid appearance are additionally Cy3-labeled for CD8b indicating a subset of lymphoyctes,

809 whereas Cy5-immunostaining of Iba (B'', color-coded in blue) is also present in apparently CD8b-

810 immunonegative cells. The overlay of staining patterns clearly demonstrates two cells co-expressing

811 both immune cell markers either containing FITC-Alb (arrow) or being devoid of FITC-Alb

812 (arrowhead). Scale bars: A'' (also valid for A, A') = 100 µm, A''' = 50 µm, B'' (also valid for B, B') = 25

813 µm, B''' = 10 µm.

814

eNeuro Accepted Manuscript

815 **Table 1**

816 Double fluorescence staining of FITC-albumin pre-labeled rat forebrain tissue sections

First primary antibodies	First visualising immunoreagents	Second primary antibodies	Second visualising immunoreagents
biotinylated mouse-anti-NeuN (1:100; Merck Millipore, Billerica, MA,USA)	Cy3-streptavidin	rabbit-anti-laminin (1:200; Dakocytomation, Hamburg, Germany)	Cy5-donkey-anti-rabbit IgG
rabbit-anti-laminin (1:400; Dakocytomation)	Cy3-donkey-anti-rabbit IgG	guinea pig-anti-GFAP (1:200; Synaptic Systems, Göttingen, Germany)	Cy5-donkey-anti-guinea pig IgG
biotinylated STL (10 µg/ml; Vector, Burlingame, CA, USA)	Cy3-streptavidin	guinea pig-anti-GFAP (1:200; Synaptic Systems)	Cy5-donkey-anti-guinea pig IgG
rabbit-anti-collagen IV (1:100; Merck Millipore	Cy3-donkey-anti-rabbit IgG	biotinylated STL (20 µg/ml; Vector)	Cy5-streptavidin
rabbit-anti-AQP4 (1:100; Alomone, Jerusalem, Israel)	Cy3-donkey-anti-rabbit IgG	biotinylated STL (20 µg/ml; Vector)	Cy5-streptavidin
rabbit-anti-AQP4 (1:100; Alomone)	Cy3-donkey-anti-rabbit IgG	guinea pig-anti-GFAP (1:200; Synaptic Systems)	Cy5-donkey-anti-guinea pig IgG
rabbit-anti-S100β (1:600; Synaptic Systems)	Cy3-donkey-anti-rabbit IgG	guinea pig-anti-GFAP (1:200; Synaptic Systems)	Cy5-donkey-anti-guinea pig IgG
rabbit-anti-Iba (1:400; Synaptic Systems)	Cy3-donkey-anti-rabbit IgG	guinea pig-anti-GFAP (1:200; Synaptic Systems	Cy5-donkey-anti-guinea pig IgG
rabbit-anti-Iba (1.200; Synaptic Systems)	Cy3-donkey-anti-rabbit IgG	biotinylated STL (20 µg/ml; Vector)	Cy5-streptavidin
biotinylated mouse-anti-CD45c (1:20; Serotec, Oxford,UK)	Cy3-streptavidin	rabbit-anti-Iba (1:200; Synaptic Systems)	Cy5-donkey-anti-rabbit IgG
biotinylated mouse-anti-CD8b (1:25; Serotec)	Cy3-streptavidin	rabbit-anti-Iba (1:200; Synaptic Systems)	Cy5-donkey-anti-rabbit IgG

817 All fluorescent immunoreagents were obtained from Dianova (Hamburg, Germany) and used at 20
818 µg/ml for 1 h. Abbreviations: NeuN – neuronal nuclei; GFAP – glial fibrillary acidic protein; STL –
819 *Solanum tuberosum* agglutinin (= potato lectin); AQP4 –aquaporin-4; Iba – ionized calcium binding
820 adapter molecule-1

eNeuro Accepted Manuscript

eNeuro Accepted Manuscript

821 **Table 2**

822 Summary of results gained by analysis of fluorescence staining after SE

Marker	Target	Colocalization with FITC-albumin?	Altered immunosignal in FITC-albumin-positive *versus* negative areas?
NeuN	Neurons	(Yes)*	n.d.
GFAP	Astroglia	No	Reduced
Iba1	Microglia	Yes	n.d.
STL	Vasculature/ endothelial cells, perivascular microglia	No	Reduced
Laminin	Vascular basement membranes of endothelium	Yes	No
Collagen IV	Vascular basement membranes of endothelium	No	Elevated
AQP4	Astroglial endfeet	No	Reduced
S100ß	Astroglial somata	No	No
CD45c	Activated microglia	No	Reduced
CD8b	Subset of T cells	Yes	No

823 AQP4, aquaporin-4, GFAP, glial fibrillary acidic protein, Iba1, ionized calcium binding adaptor
824 molecule 1, n.d., not determined, NeuN, neuronal nuclei, STL, *Solanum tuberosum* lectin; *but
825 predominantly in NeuN-immunonegative cells displaying neuronal morphology

826

eNeuro Accepted Manuscript

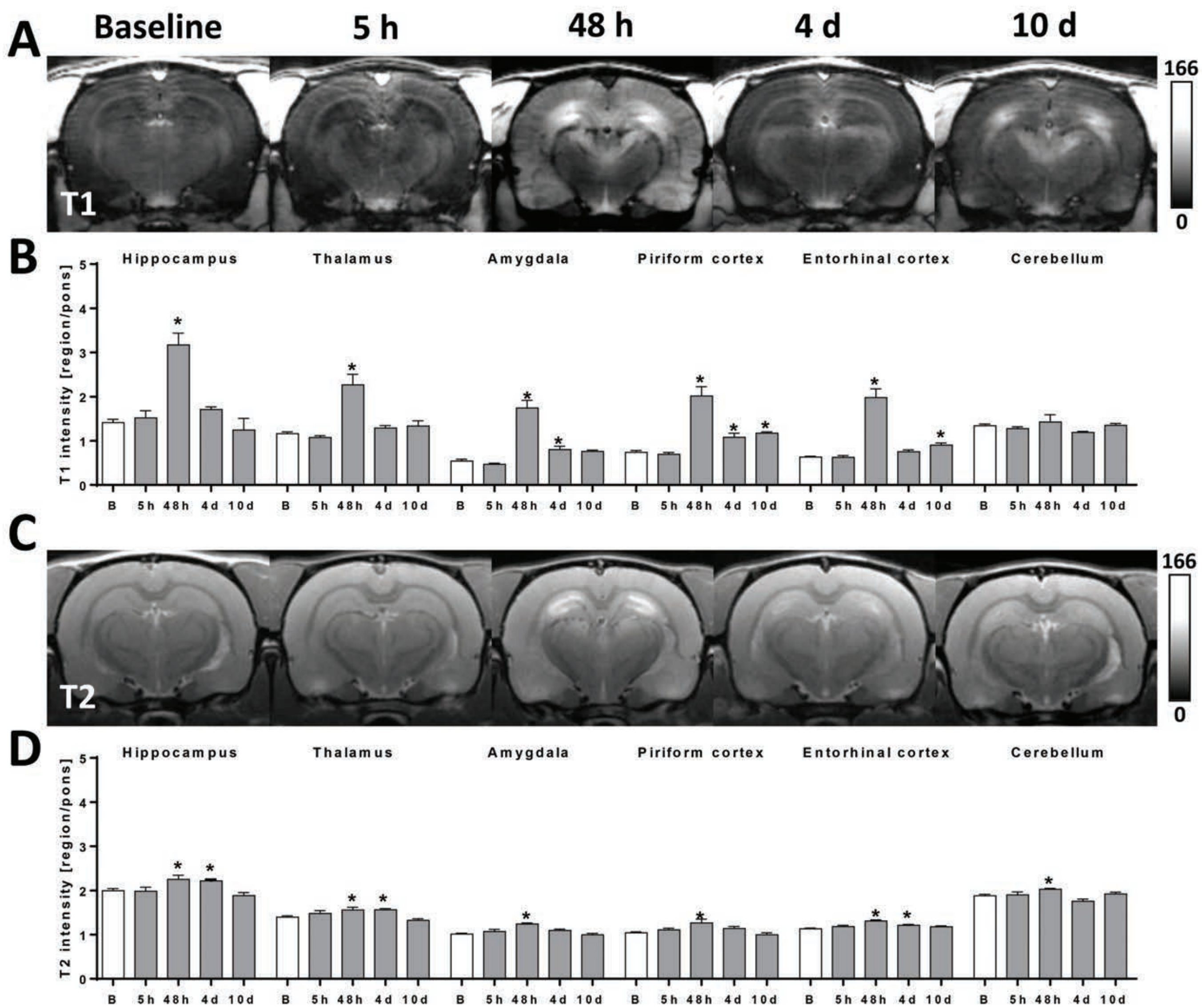

eNeuro Accepted Manuscript

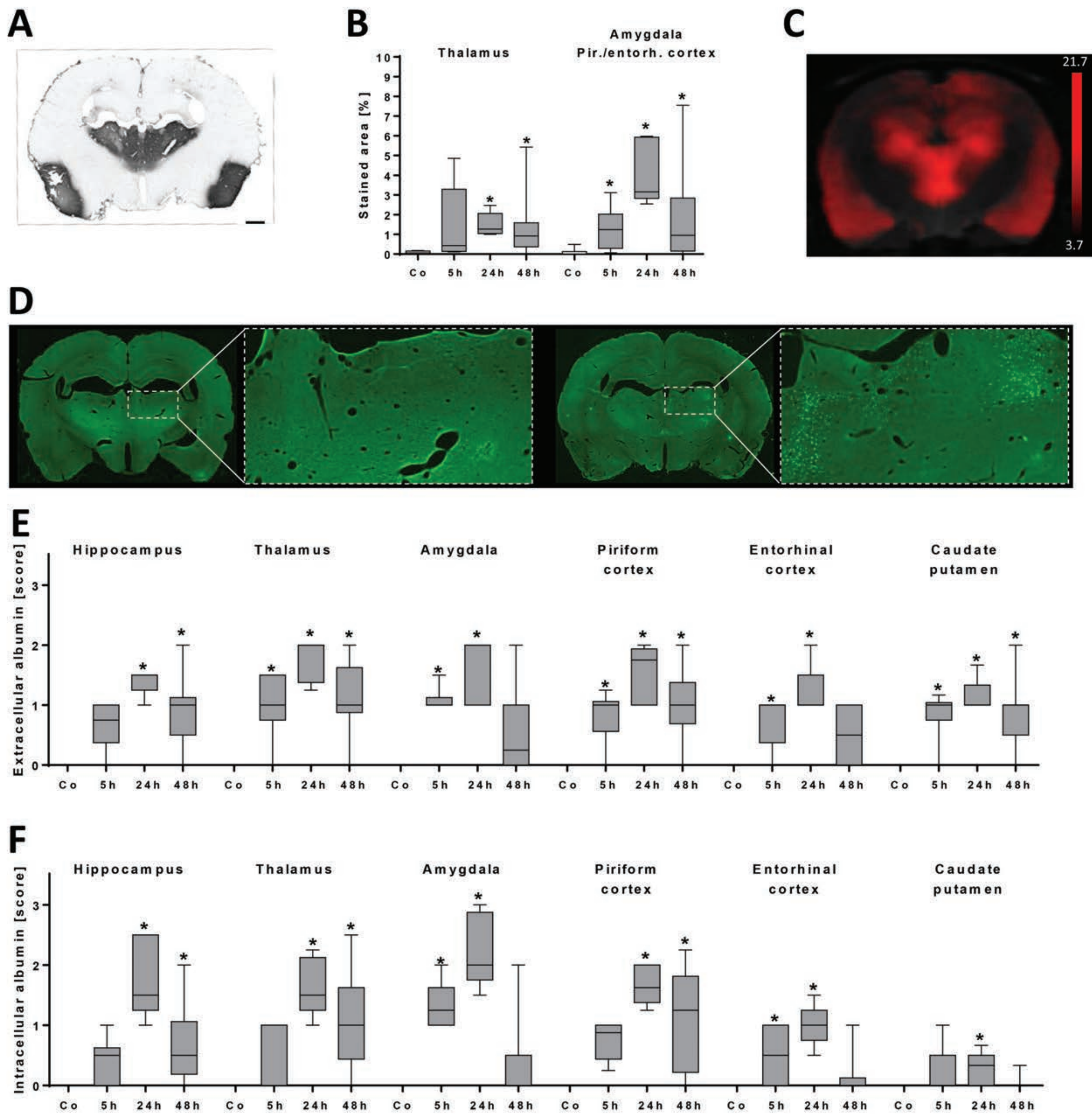

eNeuro Accepted Manuscript

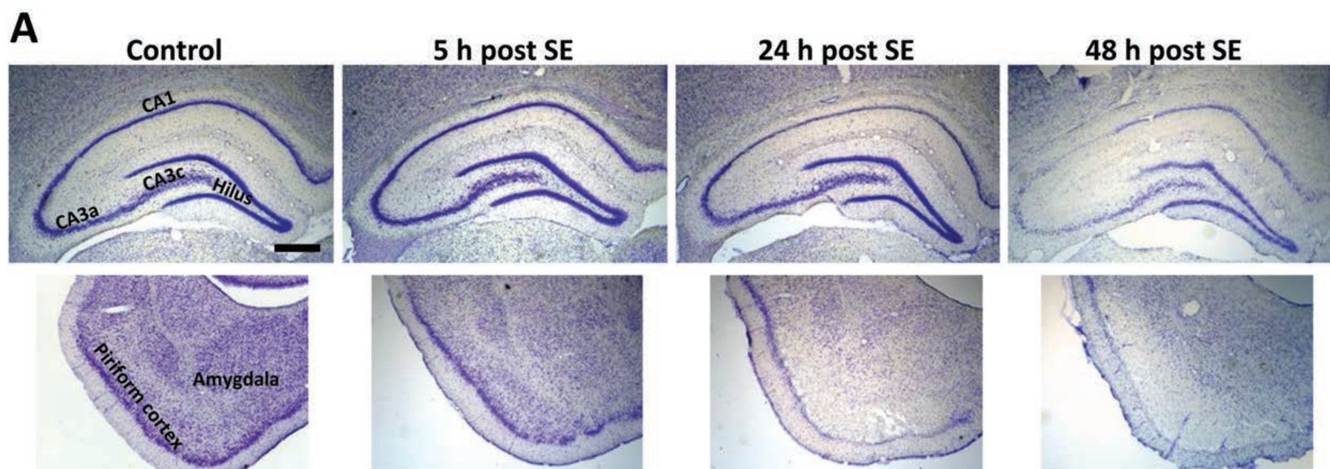

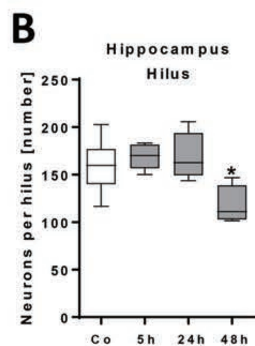

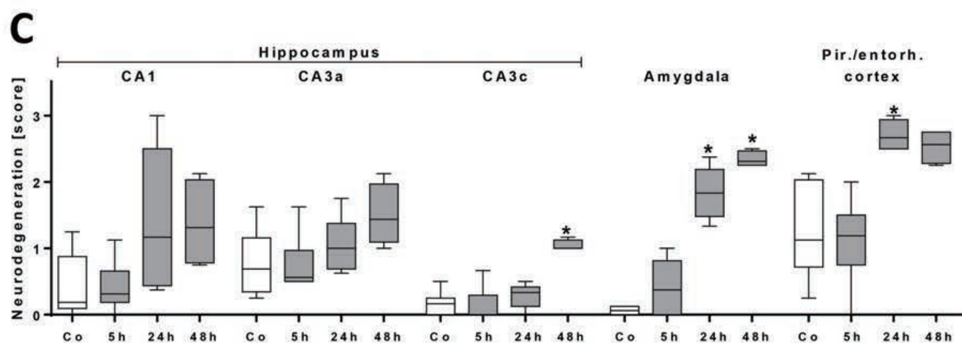

eNeuro Accepted Manuscript

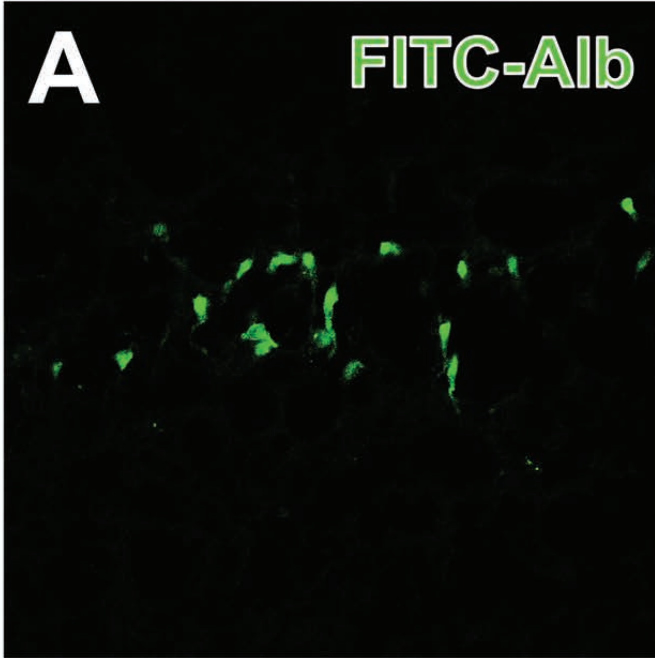

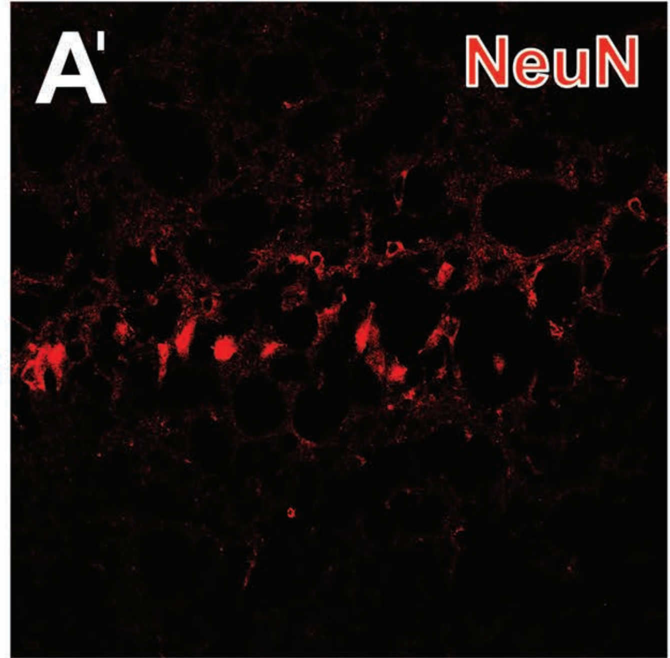

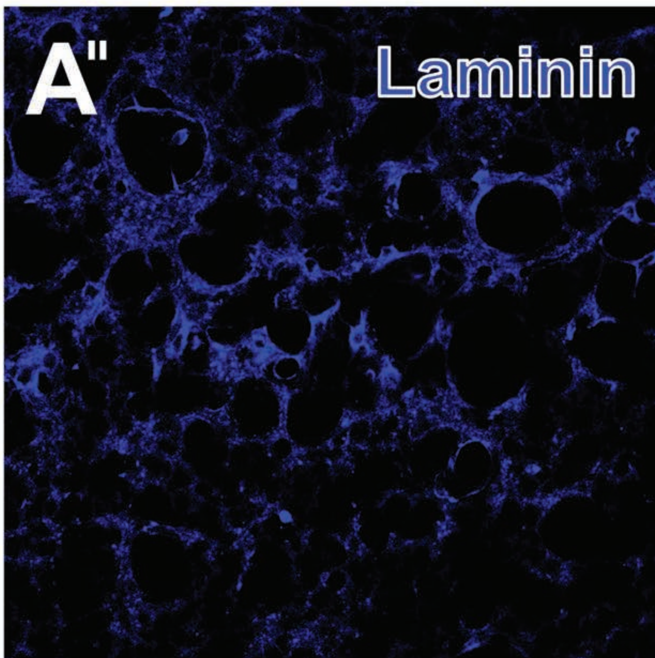

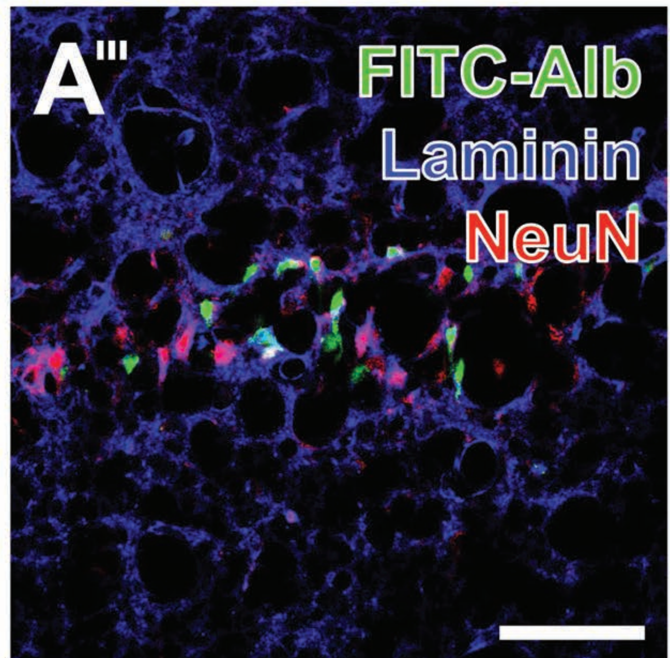

eNeuro Accepted Manuscript

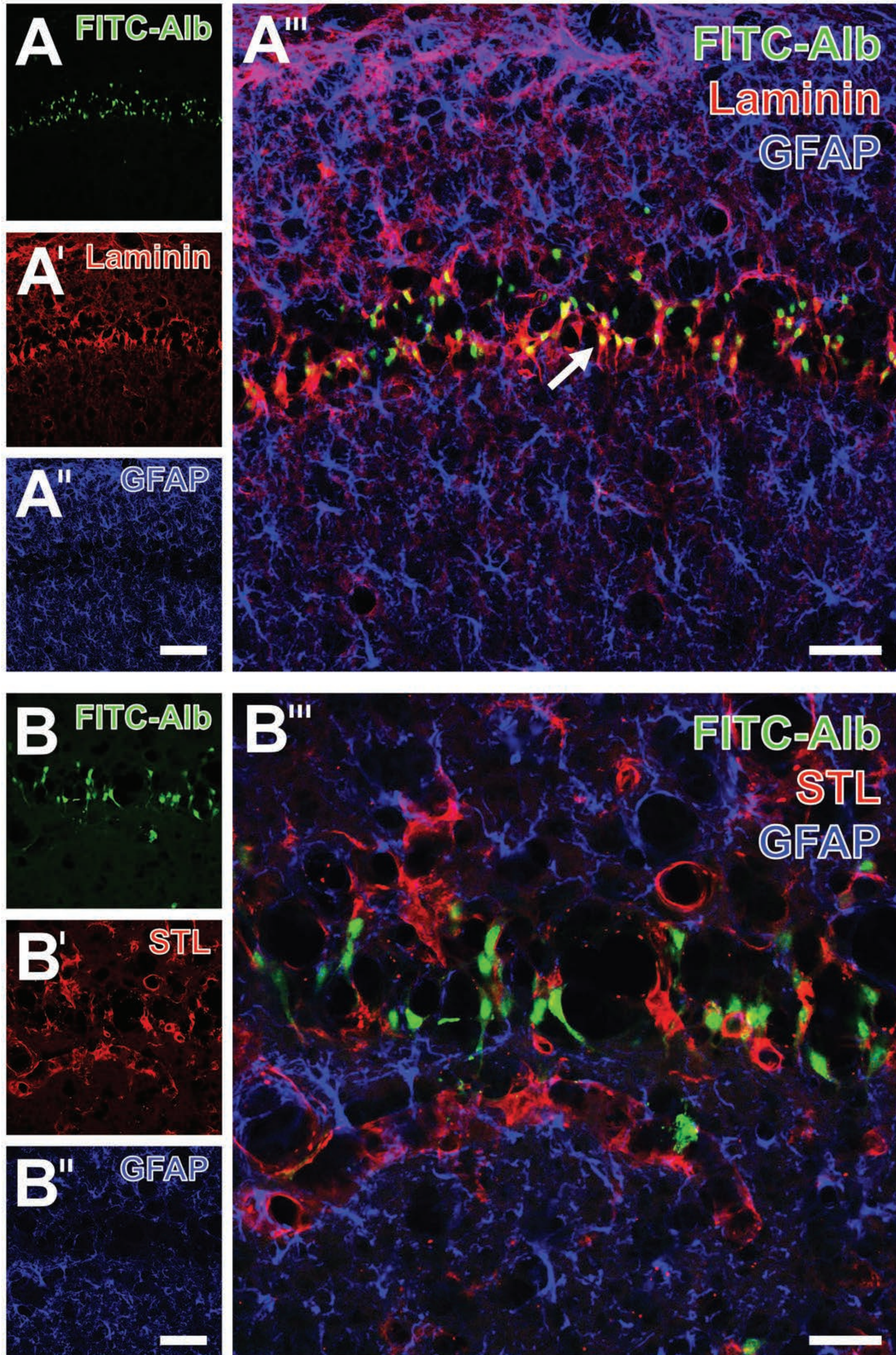

eNeuro Accepted Manuscript

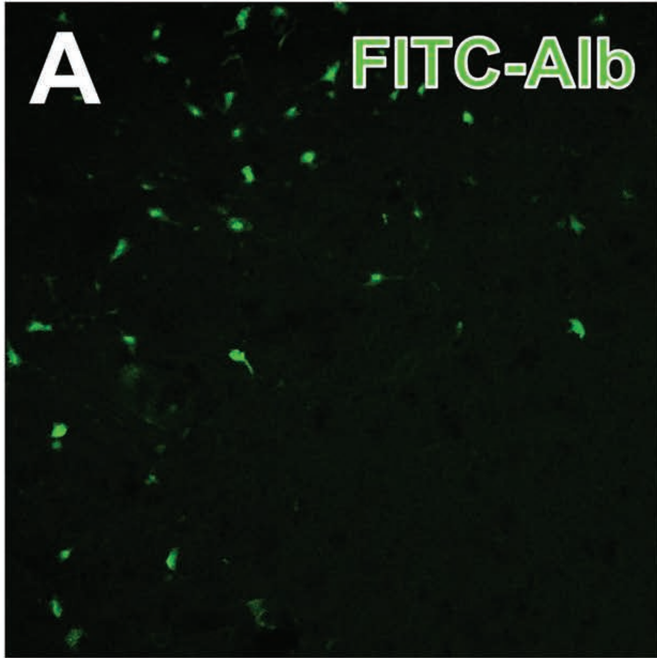

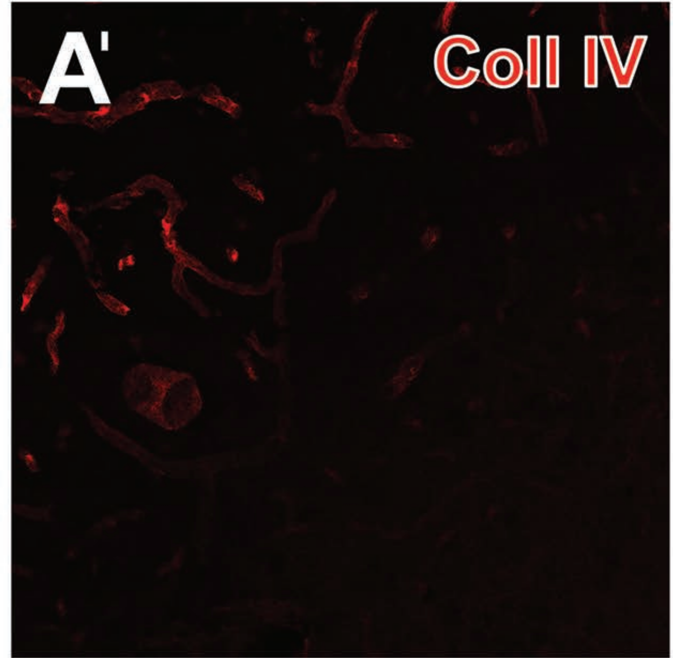

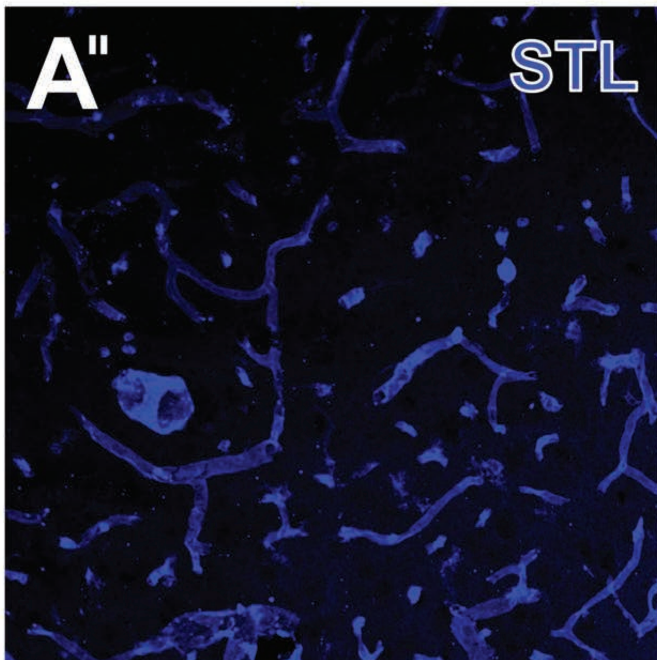

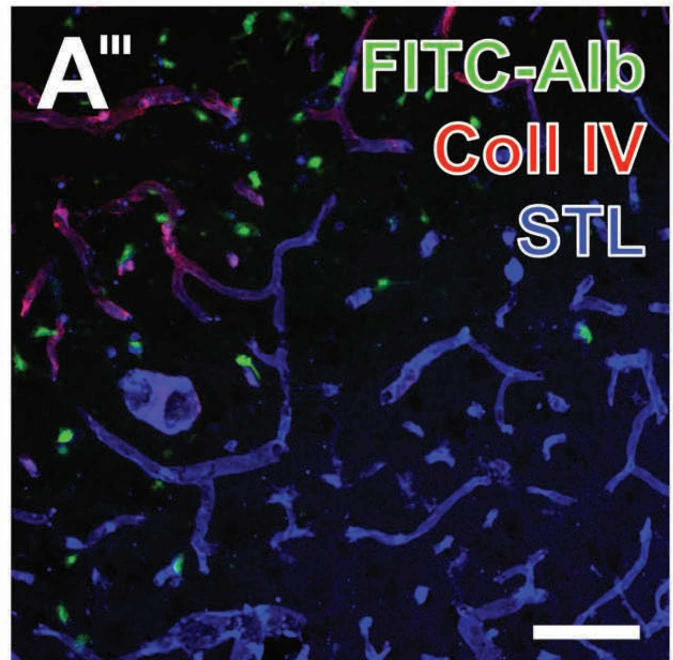

eNeuro Accepted Manuscript

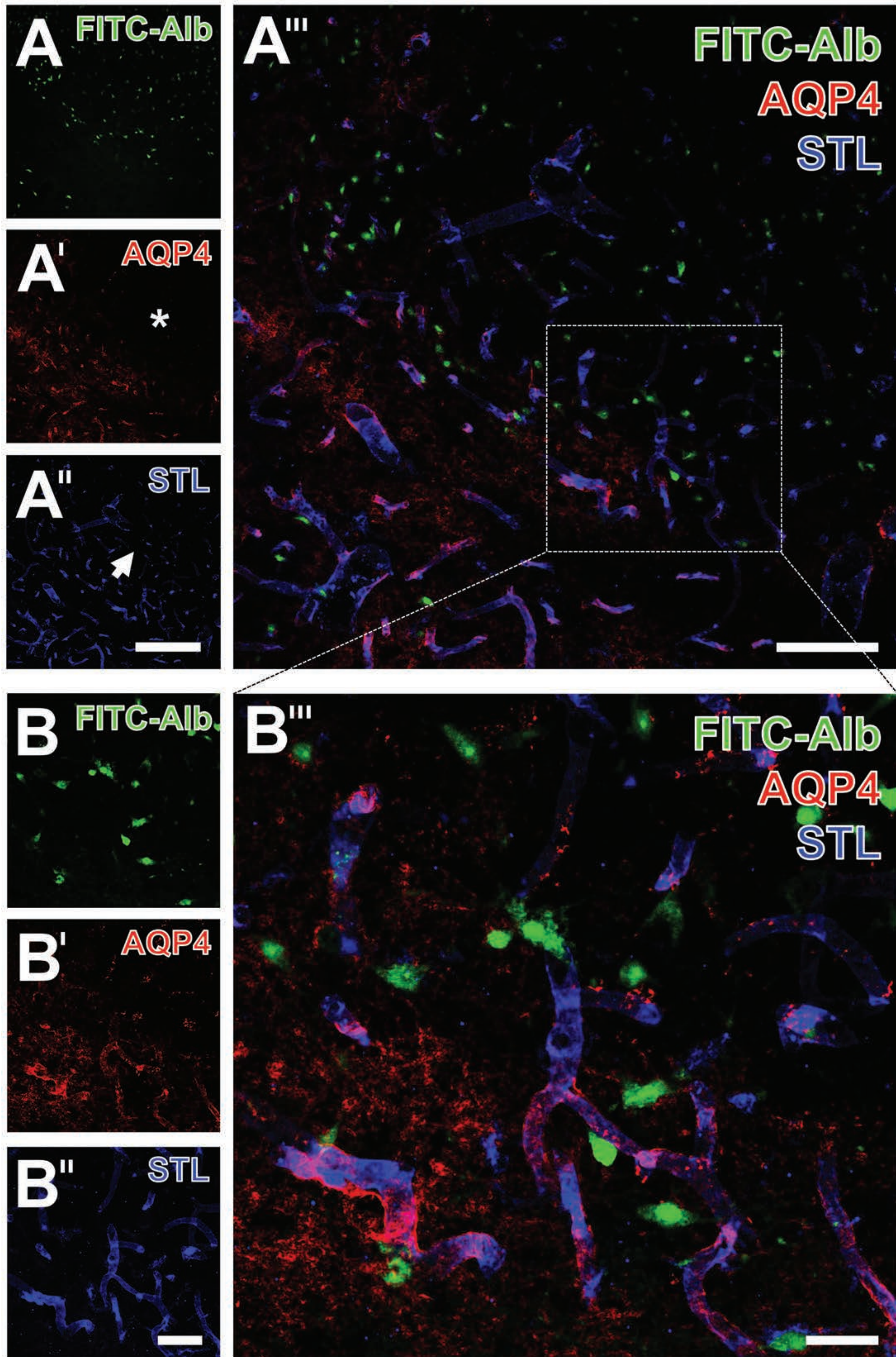

eNeuro Accepted Manuscript

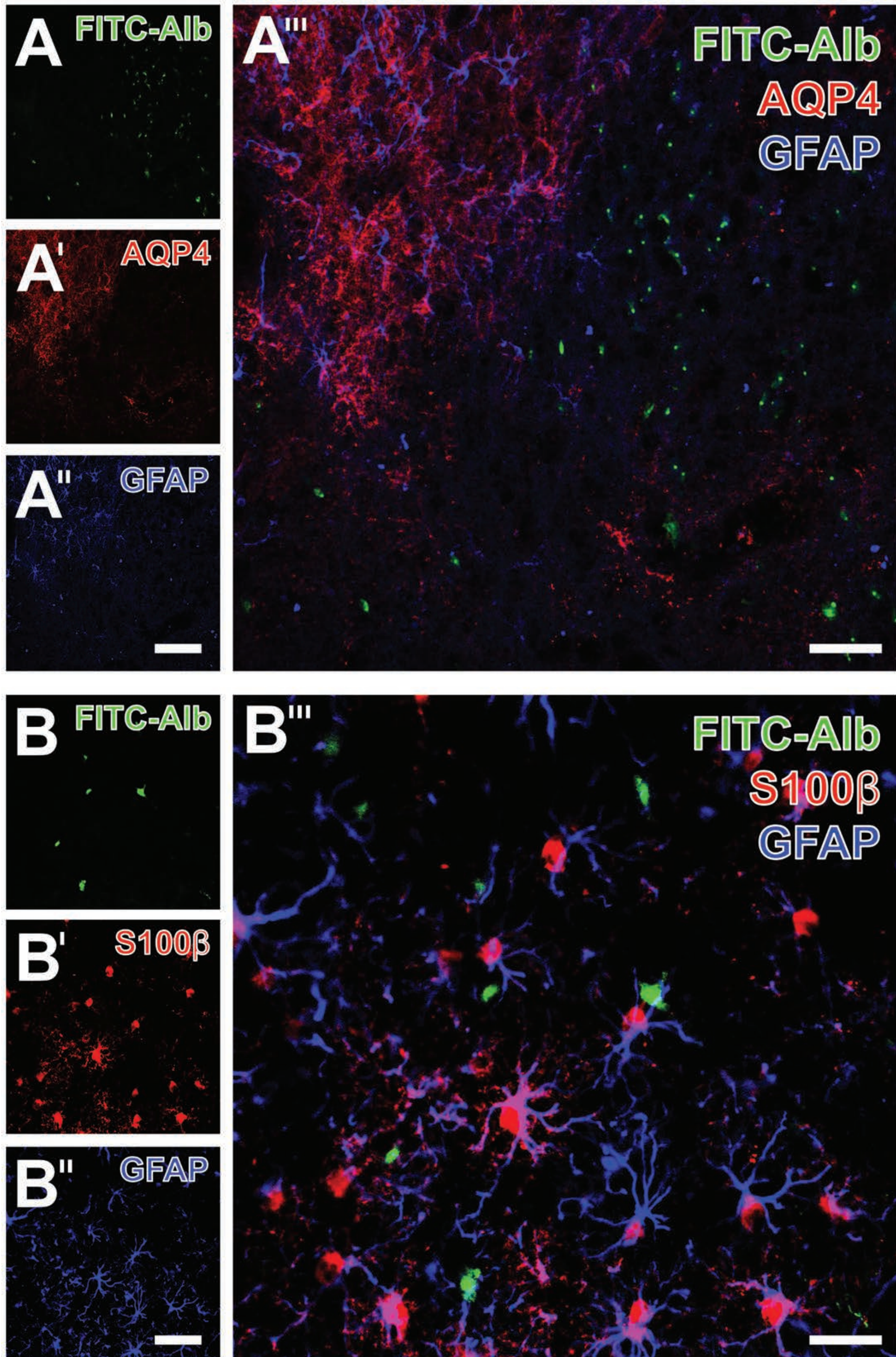

eNeuro Accepted Manuscript

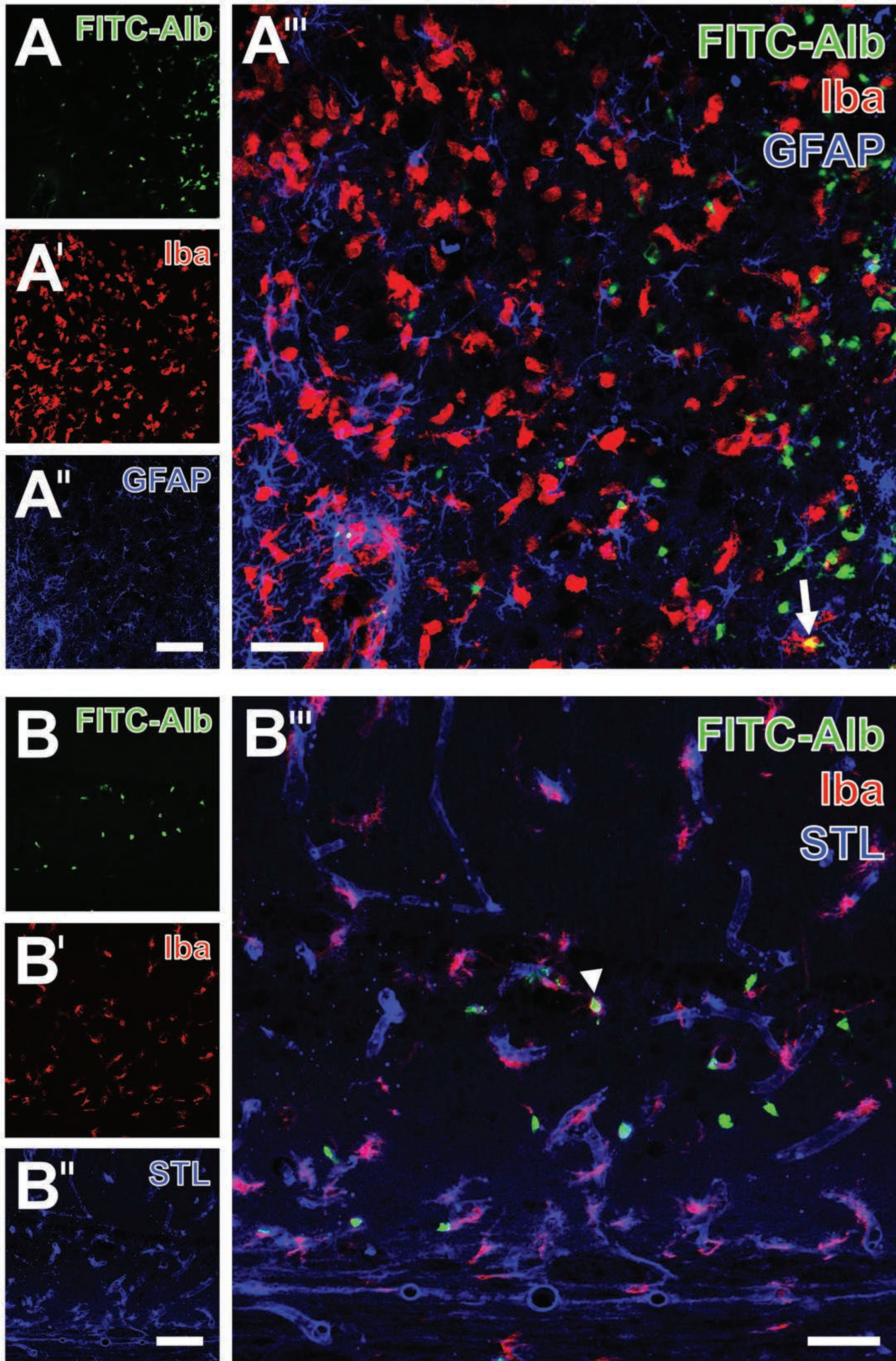

eNeuro Accepted Manuscript